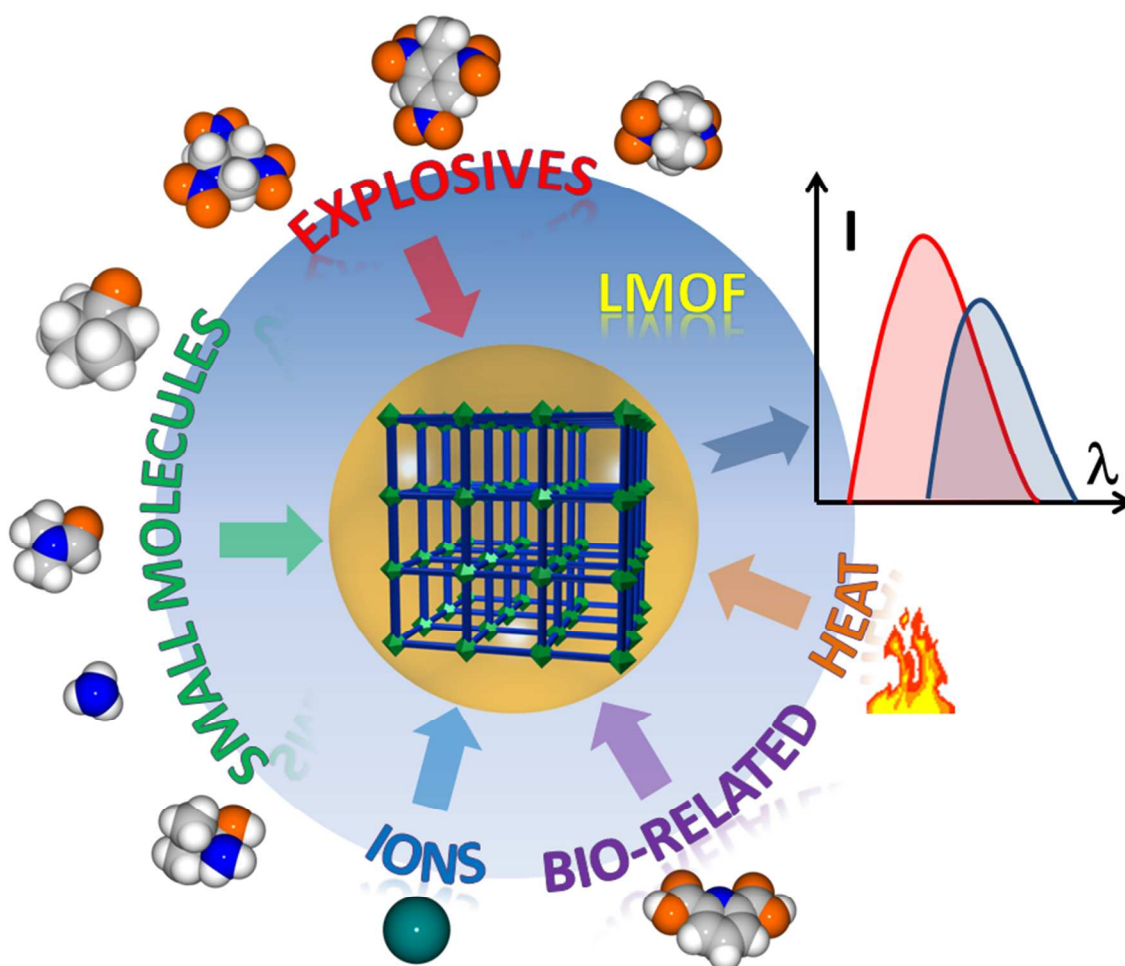




Luminescent Metal-Organic Frameworks for Chemical Sensing and Explosive Detection

| | |
|-------------------------------|--|
| Journal: | <i>Chemical Society Reviews</i> |
| Manuscript ID: | CS-REV-01-2014-000010.R1 |
| Article Type: | Review Article |
| Date Submitted by the Author: | 14-Feb-2014 |
| Complete List of Authors: | Hu, Zhichao; Rutgers University, Chemistry and Chemical Biology Deibert, Benjamin; Rutgers University, Chemistry and Chemical Biology Li, Jing; Rutgers University, Chemistry and Chemical Biology |
| | |



This review provides an update on the photoluminescence properties of LMOFs and their utility in chemical sensing and explosive detection.

ARTICLE

Luminescent Metal-Organic Frameworks for Chemical Sensing and Explosive Detection

Cite this: DOI: 10.1039/x0xx00000x

Zhichao Hu, Benjamin J. Deibert, and Jing Li*

Received 00th January 2014,
Accepted 00th January 2014

DOI: 10.1039/x0xx00000x

www.rsc.org/

Metal-organic frameworks (MOFs) are a unique class of crystalline solids comprised of metal cations (or metal clusters) and organic ligands that have shown promise for a wide variety of applications. Over the past 15 years, research and development of these materials have become one of the most intensely and extensively pursued areas. A very interesting and well-investigated topic is their optical emission properties and related applications. Several reviews have provided a comprehensive overview covering many aspects of the subject up to 2011. This review intends to provide an update of work published since then and focuses on the photoluminescence (PL) properties of MOFs and their possible utility in chemical and biological sensing and detection. The spectrum of this review includes the origin of luminescence in MOFs, the advantages of luminescent MOF (LMOF) based sensors, general strategies in designing sensory materials, and examples of various applications in sensing and detection.

Department of Chemistry and Chemical Biology, Rutgers University
610 Taylor Rd., Piscataway, NJ 08854
Fax: (+1) 732-445-5312
E-mail: jingli@rutgers.edu

1. Introduction

Metal-organic frameworks (MOFs) are a fascinating material class that are both fundamentally important and technologically relevant. They have been extensively studied for their rich



Zhichao Hu was born and raised in Tianjin, China. He obtained his B.S. in chemistry from Nankai University prior to his arrival at Rutgers in 2008. He is currently pursuing a Ph.D. in chemistry under the guidance of Prof. Jing Li. His primary interests are in the design, synthesis, and characterization of luminescent metal-organic

frameworks and their application as phosphors and chemical sensors. He also uses Density Functional Theory computations to study the electronic properties of luminescent materials and analyte-sensor interactions from a theoretical perspective.



Benjamin J. Deibert joined the Jing Li Research Group in 2011 as an undergraduate researcher, focusing on the catalytic and luminescent properties of metal-organic frameworks. Upon earning his B.A. in chemistry from Rutgers in 2012, he was accepted into the Ph.D. program of the Department of Chemistry and Chemical Biology to

continue his work in the Li Group. His current research is primarily on the synthesis and applications of metal-organic frameworks towards cleaner energy applications and environmental technologies. In 2013 he was awarded and is currently supported by the Rutgers Excellence Fellowship.

structural chemistry¹⁻⁵ and potential applications in numerous areas,^{6, 7} including but not limited to, gas storage,⁸⁻¹⁰ gas separation,¹¹⁻¹⁵ heterogeneous catalysis,¹⁶⁻²⁰ chemical sensing,²¹⁻²⁵ optoelectronics (ferroelectrics, non-linear optics, and LEDs),²⁶⁻³⁰ energy storage and conversion (batteries and solar cells),³¹⁻³⁶ drug delivery and bio-imaging.³⁷⁻³⁹ MOFs, as indicated by the name, are crystalline solids constructed via self-assembly of single metal cations (primary building unit or PBU) or metal clusters (secondary building unit or SBU) and organic ligands having multiple binding sites, forming one, two, or three dimensional extended coordination networks.⁴⁰ The organic ligands often contain aromatic or conjugated π moieties that are subject to excitation, giving rise to optical emission or photoluminescence (PL) upon irradiation. In addition, the metal components can also contribute to photoluminescence, in which case lanthanides⁴¹ or various inorganic clusters⁴²⁻⁴⁶ are often involved. Naturally, these properties of luminescent MOFs (LMOFs) can potentially be used for real-world applications. The PL in LMOFs can be utilized conveniently; often it does not require the fabrication of thin films, which, while proven possible in some cases, can be challenging with respect to the general pool of these materials.^{47, 48} Thanks to modern technology and state-of-the-art instrumentation, efficient, economic, and portable fluorimeters are readily available, greatly promoting research and development in this subject area.

Given the nearly limitless choices of metal and ligand combinations, MOFs thrive on structural diversity and tunable chemical and physical properties. The intrinsic permanent porosity in a large number of MOFs further enables the adsorption of guest molecules and therefore enhances host-guest interactions, since the pore size and shape, chemical composition and surface environment within the pores can be finely controlled, and therefore, the selective seizing of certain guest molecules is often times achieved. This merit of MOFs is the foundation of many well explored applications, especially in gas storage and separation. Additionally, the perturbation from adsorbed guest molecules can alter LMOFs' photoemission profiles, making them excellent candidates for c h e m o s e n s i n g .

renewable energy applications. She published > 250 publications. She currently serves as Associate Editor for Journal of Solid State Chemistry.



Jing Li received her Ph.D. degree from Cornell University in 1990 under the guidance of Professor Roald Hoffmann. After two years of postdoctoral work with Professor Frank DiSalvo (Cornell) she joined the chemistry faculty at Rutgers University in 1991 as Assistant Professor. She was promoted to Associate Professor in 1996, Full Professor in 1999, and

Distinguished Professor in 2006. Her research is primarily on the development of functional materials that are both fundamentally important and potentially useful for clean and

The advantages and challenges of LMOF based luminescence sensors are well summarized by several previous review articles.^{21, 23, 24} A comprehensive list of LMOFs was provided by Cui and coworkers in their 2011 review article that we have sought to continue in this work,²³ hence Table 1 lists the LMOFs reported since then that have been investigated for sensing applications as well as those demonstrating interesting or potentially useful luminescence properties. In the following sections we aim to provide an update and summary on this ever-expanding field of LMOF research in the past three years.

1.1. The Origin of Luminescence in LMOFs

Luminescence can be defined as the emission of light upon absorption of energy under the condition that the energy source is not heat based, which refers to incandescence.^{21, 23, 49, 50} There are two main types of luminescence: fluorescence, which is a spin-allowed radiative transition from the lowest singlet excited state S_1 of the fluorophore to its singlet ground state S_0 ; and phosphorescence, which refers to the spin-forbidden radiative transition from the triplet state T_1 to ground state S_0 .^{21, 23, 49, 50} Photoluminescence initiated by photo-excitation is one type of luminescence that is extensively discussed in this review.²¹ Luminescence in MOFs generally arises from the building components: conjugated organic ligands and/or metal ions or clusters, although in some cases adsorbed guest molecules may also contribute to the emission. Organic linkers with aromatic moieties or extended π systems are commonly used in the construction of porous MOFs due to their rigid molecular backbone. The π electrons in these linkers contribute greatly to luminescence, which can be classified as linker based luminescence or ligand-to-ligand charge transfer (LLCT). As the organic fluorophores are immobilized in an ordered arrangement and in close proximity with one another in a MOF structure, the nature of their intermolecular communication can be altered resulting in photoemissions that are different from their free form.⁵¹ Ligand to metal charge transfer (LMCT) and metal to ligand charge transfer (MLCT) are also common among d^{10} transition metal based MOFs: LMCT is often observed in Zn (II) and Cd (II) compounds,^{52, 53} while MLCT is generally seen in Cu (I) and Ag (I) compounds.^{45, 54} It should be noted that these mechanisms are not mutually exclusive; more than one emission pathway can coexist in a competitive manner with another. Metal-centered luminescence is often found in lanthanide MOFs. Strongly photon absorbing linkers with efficient intersystem crossing are preferred in constructing lanthanide LMOFs because they ensure the delivery of excitation energy from their triplet excited states to the emissive states of lanthanides through an antenna effect.^{21, 41}

1.2. Utilizing the Optical Signals of LMOFs

The permanent porosity of MOFs makes them stand out as a unique family of functional materials. Their intrinsically porous structures harbor nearly all of the major applications developed for this material class, many of which take advantage of the adsorption of guest molecules within the cavity of the framework. The capture of guest molecules in the pores allows

them to be in close proximity with the organic walls or metal centers of the host structure, and thus, readily interact with the MOF. The perturbation induced by these guest molecules can alter multiple aspects of the physicochemical properties of the captor, including light absorption and emission profiles. Color change that is visible to the naked eye is arguably the most preferred signal for sensing, simply because it does not require instrumentation and represents the most convenient method of detection. In some cases, performing an exchange of solvent guest molecules will shift the emission spectrum and tune the color of the compound. Identification of a guest molecule can be realized by utilizing a guest-dependent color change. Some ionic species are also known to have a similar colorimetric effect.⁵⁵⁻⁵⁷

For LMOFs, in principle any change in their spectroscopic characteristics can potentially be used as a sensing signal, while the most commonly observed change is the fluorescence intensity. Depending on the electronic nature of the molecule being detected (also referred to as the analyte), either quenching or enhancement of the luminescence can occur. This can be attributed to either electron transfer or energy transfer between the analyte molecule and the LMOF, or a combination of the two.^{49, 58-66} Nitroaromatics, which are exemplary explosives or explosive-like molecules, are known as strong quenchers owing to their high electron affinity.^{59, 61, 62, 67} Paramagnetic metal ions, such as Mn^{2+} , Co^{2+} , Ni^{2+} , and Cu^{2+} , are also capable of quenching fluorescence since they can induce LMCT and relax the excitation energy through a non-radiative pathway.^{21, 68, 69} On the other hand, electron rich species, such as benzene and its derivatives with electron donating substituents, can enhance fluorescence, possibly due to their ability to donate an electron from an excited state to the LUMO or conduction band (CB) of the LMOF.^{62, 70-73}

Another method of luminescence sensing is “turn-on” detection, where the capture of an analyte molecule results in the shift of an emission peak or a new emission peak (typically in the visible range) evolving from a previously dark background.⁷⁴⁻⁷⁶ For example, the selective binding of analyte molecules can trigger a strong emission of an originally low-emitting or non-emitting MOF, which is known as guest induced emission.⁷⁵ Focusing on the shifting of emission peaks or the evolution of a new peak has several advantages: first, monitoring the evolution of a new emission peak is more sensitive than comparing the changes in emission intensity of the same peak, which may translate to lower detection limits. Second, intensity change of an emission is not always specific; molecules of similar electronic properties tend to affect intensity in a similar fashion. For example, nitroaromatics can all act as strong quenchers, and as such, judging solely by the changes in fluorescence intensity is often insufficient for identifying the individual nitroaromatic species. However, the host material can be designed to have strong interactions with a particular analyte molecule resulting in an additional energy shift of the emission peak. With the aid of this additional signal, more accurate identification of analyte molecules can be achieved. The guest-host chemistry involved in these processes

is intriguing, and understanding this interaction is fundamental and vital to designing LMOFs with high selectivity and sensitivity for sensing applications.

1.3. The Advantages of Using MOFs as Sensory Materials

LMOFs are often compared with organic conjugate polymers when evaluating their performance as sensory materials. Their crystalline nature, diverse and easily modifiable structures and topology, permanent porosity, systematically tunable band gaps and electronic structures, and a wide range of physicochemical properties all highlight some of their advantages. Most notably, the sustainable pores within LMOFs provide a natural habitat for guest molecules. The capture of guest molecules within the pores not only increases the chances of guest-host interactions, but also pre-concentrates the guest molecule, which may be responsible for sensitive detection.^{21, 24} In addition, functional groups within the framework, such as Lewis acidic or basic sites in the ligands, and/or open metal sites, further promote preferred analyte binding for selective detection. Thirdly, the electronic properties of an LMOF structure may be fine-tuned. For example, given the same metal center and network connectivity, band gaps can be varied by changing the size of the SBU and the degree of conjugation of the organic linkers.⁷⁷ Needless to say, changes to a framework's metal centers or their connectivity also lead to changes in band gaps and atomic compositions of the valence band (or HOMO) and/or conduction band (or LUMO). Such

tunability is crucial for sensing applications as it directly relates to the optical absorption and emissions properties. Fourthly, immobilization of organic linkers in a rigid framework can potentially reduce non-radiative relaxation caused by free rotation and vibration of the linker, and therefore lead to stronger emissions.⁷⁸⁻⁸⁰ Aggregation induced emission (AIE) is a perfect example: a low-emissive linker when in a dilute solution may exhibit strong fluorescence upon assembly into a rigid MOF structure.⁵¹ Furthermore, MOFs generally have relatively high thermal-stability, and it is not uncommon for them to remain crystalline at a few hundred degrees Celsius. Fluorescent conjugate polymers typically lose their emission at elevated temperatures, especially upon melting or glassifying. Several MOFs have been reported to maintain their fluorescence at relatively high temperatures, and thus it becomes possible to utilize their fluorescence when a specific analyte's binding requires an elevated temperature.⁷⁴ Last but not the least, compared to amorphous materials, the highly ordered crystalline samples of MOFs allow precise and easy identification and characterization of their structures (e.g. by X-ray diffraction methods), making them perfect systems for investigating structure-property correlations and host-guest interactions. This merit has significant implications in both applications and fundamental studies. Overall, LMOFs have great potential as a unique class of sensory materials.

1.4. Strategies for Designing LMOF Sensors

Table 1. Selected list of LMOFs, excitation and emission wavelengths, and reported luminescence applications.

| Metal | MOF | λ_{ex} (nm) | λ_{em} (nm) | Ref | Application |
|---|--|----------------------------|----------------------------|-------------------------------|--|
| Li | $\{\text{Li}_3[\text{Li}(\text{DMF})_2](\text{cpma})_2\} \cdot 4\text{DMF} \cdot \text{H}_2\text{O}$ | 345 | 430 | 81 | Explosive sensing |
| Mg | $\text{Mg}(\text{dhdcc})$ | 365 | ~500 | 74 | NH_3 sensing |
| | $[\text{Mg}(\text{dht})] \cdot (\text{DMF})_2$ | 370 | ~480 | 68, 82 | Tunable emission, Cu^{2+} sensing |
| Al | $[\text{Al}(\text{OH})(\text{ndc})(\text{DMF})_{1.5}(\text{H}_2\text{O})_{1.5}] \cdot n\text{G}$ | 350 | ~390, 400, 525 | 83 | Small molecule sensing |
| Cu | $[\text{Cu}_4\text{I}_4(\text{Cu}^{\text{I}}_6)_2(3\text{-ptt})_{12}] \cdot 24\text{DEF} \cdot 12\text{H}_2\text{O}$ | 275 | 770, 800 | 46 | Thermochromic, dual emissive |
| | $[(\text{CuCN})_3\text{L}^1(\text{guest})_x]_n$ $x = 1$ or 2 | 320 | ~450 | 84 | VOC sensing |
| | Cu-tca | 350 | ~430 | 85 | NO bio sensing |
| | $[\text{Cu}_4\text{I}_4(\text{dabco})_2]$ | 350 | 588 | 43 | Cu_4I_4 cluster emission |
| Cu-Mn | $[\text{Cu}_4\text{I}_4(\text{NH}_2\text{CH}_3)\text{Cu}_3(\text{L}^2)_3]$ | 370 | 524, 641 | 86 | Thermochromic emission |
| | $[\text{Cu}_4\text{I}_4\text{Cu}_3(\text{L}^3)_3]$ | 370 | 556 | 86 | Thermochromic emission |
| | $\text{MV}[\text{Mn}_2\text{Cu}_3(\text{mpba})_3(\text{H}_2\text{O})_3] \cdot 20\text{H}_2\text{O}$ | 225, 400 | 330, 544 | 87 | Small molecule sensing |
| | $\text{Zn}_4\text{O}(\text{L}^4)_{1.5}$ | - | - | 88 | Ln encapsulation, tunable emission |
| Zn | $[\text{Zn}_3(\text{L}^5)(\text{H}_2\text{O})_2] \cdot 3\text{DMF} \cdot 7\text{H}_2\text{O}$ | - | - | 89 | Ln encapsulation, tunable emission |
| | $[\text{Zn}_3(\text{tatb})_2(\text{H}_2\text{O})_2]$ | NS | 423 | 90 | DMA enhanced luminescence |
| | $[\text{Zn}_8(\text{ad})_4(\text{bpdc})_6\text{O} \cdot 2\text{Me}_2\text{NH}_2 \cdot 8\text{DMF} \cdot 11\text{H}_2\text{O}]$ | 280/385 | 340/415 | 91 | Ln encapsulation in water, NIR emission |
| | $[\text{Zn}_2(\text{tib})(\text{HL}^6)(\text{H}_2\text{L}^6)_{0.5}] \cdot 2\text{H}_2\text{O}$ | 245 | 394 | 92 | Nitroaromatic sensing |
| | $[\text{Zn}_2(\text{tib})(\text{L}^7)] \cdot \text{H}_2\text{O}$ | 245 | 394, 495, 550 | 92 | Nitroaromatic sensing |
| | $\text{Zn}_3(\text{L}^8)_2(\text{L}^9)$ | 246 | 326, 392 | 93 | Small molecule sensing, nitrobenzene sensing |
| | $[\text{Zn}_3(\text{tib})(\text{btc})_2(\text{H}_2\text{O})_6] \cdot 2\text{H}_2\text{O}$ | 277 | 354 | 92 | Nitroaromatic sensing |
| | $[\text{Zn}_{1.5}(\text{L}^{10})(\text{H}_2\text{O})] \cdot 1.5\text{BZ}$ | 280 | 390 | 94 | Explosive sensing |
| | $[\text{Zn}_2(\text{oba})_2(\text{bpy})] \cdot \text{DMA}$ | 280 | 420 | 62 | Explosive sensing |
| | $[\text{Zn}(\text{oca-OH})_2(4,4'\text{-bipy})_{0.5}]$ | 286 | ~475 | 95 | Small molecule sensing |
| | $[\text{Zn}_2(\text{tcpe})(\text{H}_2\text{O})_2] \cdot 4\text{DEF}$ | 296 | 480 | 51 | Small molecule sensing |
| | $[\text{Zn}_2(\text{bpdc})_2(\text{bpee})]$ | 300NS | 420 | 96 | Explosive sensing |
| | $\text{Zn}_3(\text{bpdc})_3(\text{bpy}) \cdot 4\text{DMF} \cdot \text{H}_2\text{O}$ (LMOF-131) | 300 | 420 | 72 | Explosive sensing |
| | $[\text{Zn}_2(\text{ndc})_2(\text{bpe})] \cdot 2.5\text{DMF} \cdot 0.25\text{H}_2\text{O}$ | 300 | ~475 | 70 | Explosive sensing, 2D Mapping |
| $[\text{Zn}_2(\text{ndc})_2(\text{bpee})] \cdot 2.25\text{DMF} \cdot 0.5\text{H}_2\text{O}$ | 300 | ~460 | 70 | Explosive sensing, 2D Mapping | |
| $[\text{Zn}(\text{ndc})(\text{bpy})_{0.5}]$ | 300 | ~450 | 71 | Explosive sensing | |
| $\text{Zn}_3(\text{bpdc})_3(2,2'\text{-dmbpy}) \cdot 4\text{DMF} \cdot \text{H}_2\text{O}$ (LMOF-132) | 320 | 388 | 72 | Explosive sensing | |
| $\text{Ag}@[\text{Zn}_2(\text{bpdc})_2(\text{bpee})] \cdot 2\text{DMF}$ | 320 | 447 | 97 | Olefin sensing | |
| $[\text{Zn}_7\text{O}_2(\text{bpdc})_4(\text{dmpp})_2] \cdot 6\text{DEF} \cdot 10\text{H}_2\text{O}$ | 323 | 390 | 98 | Nitrobenzene sensing | |
| $[\text{Zn}(\text{bpe})(\text{bdc})] \cdot 4\text{H}_2\text{O}$ | 325 | 470 | 99 | Water sensing | |
| $\text{Zn}_2(\text{bpdc})_2(\text{bpe}) \cdot 2\text{DMF}$ (LMOF-141) | 330 | 450 | 72 | Explosive sensing | |
| $\text{Zn}(\text{bpdc})(\text{bpe}) \cdot \text{DMF}$ (LMOF-151) | 330 | 425 | 72 | Explosive sensing | |
| $[\text{Zn}(\text{ndc})(\text{bpe})_{0.5}]$ | 330 | ~425 | 71 | Explosive sensing | |
| $[\text{Zn}(\text{ndc})(\text{bpee})_{0.5}]$ | 330 | ~450 | 71 | Explosive sensing | |

| | | | | | |
|-------|--|---------------|------------------------------|-----|--|
| | $[\text{Zn}_3(\text{OH})_2(\text{btca})_2] \cdot 2\text{H}_2\text{O}$ | 340 | 425 | 100 | Aromatic sensing |
| | $[\text{Zn}_7(\text{L}^{11})_3(\text{H}_2\text{O})_7]_n \cdot [\text{Zn}_5(\text{L}^{11})_3(\text{H}_2\text{O})_5]_m$ | 340 | 430 | 101 | I ₂ sensing |
| | $\text{Zn}(\text{HCOO})_2(\text{L}^{12})$ | 340 | 422, 485, 514 | 102 | Excitation tunable green/blue phosphorescence |
| | $[\text{Zn}(\text{ndc})(\text{ted})_{0.5}]$ | 340 | ~420 | 71 | Explosive sensing |
| | $\text{Zn}_2(\text{tcpe})$ | 350 | ~500 | 74 | NH ₃ sensing |
| | $[\text{Zn}_4\text{O}(\text{L}^{13})_2(\text{H}_2\text{O})_3] \cdot 3\text{DMA} \cdot 3\text{EtOH} \cdot 6\text{H}_2\text{O}$ | 350 | 470 | 103 | Explosive sensing (I) |
| | $[\text{Zn}_2(\text{L}^{14})(\text{H}_2\text{O})] \cdot (\text{NO}_3) \cdot \text{DMF}$ | 350 | 402 | 104 | Ln and I ₂ sensing and encapsulation |
| | $\text{Alq}_3 @ [\text{Zn}_{16}(\text{L}^{15})_3(\text{H}_2\text{O})_{16}] (\text{NO}_3)_8 \cdot x\text{G}$ | 360 | ~500 | 105 | Chromophore guest tunable emission |
| | $\text{Zn}_4\text{O} \cdot (\text{L}^{16})_3 \cdot (\text{DEF})_2 \cdot (\text{H}_2\text{O})_2$ | 360 | ~520 | 55 | Pd ²⁺ sensing |
| | Zn-BCPA | 370 | 438 | | Explosive sensing |
| | $\text{Zn}(\text{L}^{17})(\text{Hbtc}) \cdot (\text{H}_2\text{O})_2$ | 370 | 424, 539 | 106 | Excitation tunable emission, white light |
| | $[\text{Zn}_3(\text{tdpat})(\text{H}_2\text{O})_3]$ | 370 | 435 | 107 | Nitrobenzene sensing (I), PL thermometer |
| | $[\text{Zn}_3(\text{cpoip})_2(4,4'\text{-bpy})_2 \cdot \text{H}_2\text{O}]$ | 377 | 448 | 108 | MeOH in EtOH sensing |
| | $[\text{Zn}_2(\text{im})_4(\text{DMF})]$ | 380 | 445 | 109 | Blue emission, white LED by mixing with yellow emitter |
| | $[\text{Zn}_2(\text{H}_2\text{dht}^*)(\text{dht}^*)_{0.5}(\text{azpy})_{0.5}] \cdot 4\text{H}_2\text{O}$ | 390 | ~530 | 110 | Small molecule sensing |
| | $[\text{Zn}_{12}(\mu_6\text{-O})_2(\text{tcomp})_4] \cdot 3\text{H}_2\text{O} \cdot 8\text{NO}_3 \cdot 8\text{DMF}$ | 390 | 579, 613 | 111 | Small molecule sensing |
| | $[\text{Zn}(\text{L}^{18})(\text{H}_2\text{O})_2] (\text{NO}_3)_2 \cdot 2\text{H}_2\text{O}$ | 394 | 541 | 56 | Anion tunable emission |
| | $\text{Zn}(\text{Meim})_2$ | 396 | ~450 | 112 | Small molecule sensing, Cd ²⁺ /Cu ²⁺ sensing |
| | $\text{A-GO/L}^{19}\text{-Zn}^{2+}$ | 410NS | ~460 | 113 | Explosive sensing |
| | $\text{Zn}(\text{L}^{20,21,22})(\text{dpb}) \cdot x\text{DMF}$ | 415, 420, 480 | 310, 300, 360 | 73 | Explosive sensing (I) |
| Zn-Mn | $[\text{Zn}_2\text{Mn}(\text{OH})_2(\text{mip})_2]$ | 320 | 737 | 114 | Ln and Mn ²⁺ tunable emission |
| Zn/Ru | $[\text{Zn}_2\text{L}^{23}(\text{C}_2\text{O}_4)_2] \cdot 2\text{DMF} \cdot 3\text{H}_2\text{O}$ | 453NS | 635 | 115 | Optical imaging |
| Zn/Ru | $[\text{Zn}_3(\text{L}^{24})_2(\mu\text{-OH})(\text{HCO}_2) \cdot \text{DMF} \cdot 2\text{H}_2\text{O}] \cdot 6\text{H}_2\text{O}$ | 485 | 655 | 116 | Phosphorescence, MV ²⁺ and MB ⁺ quenching |
| Y | $[\text{Y}_3(\text{OH})_6(\text{HCO}_2)_3(\text{CO}_3)_2(\text{C}_4\text{O}_4)] \cdot 2.5\text{H}_2\text{O}$ | 420 | 512 | 117 | Intrinsic green phosphor, Eu ²⁺ doping, white light |
| Zr | Zr-dmbd | 355 | ~500 | 118 | Hg sensing |
| | Zr-ndc | 360 | 411 | 119 | Small molecule sensing |
| | $\text{Zr}_6(\mu_3\text{-O})_4(\mu_3\text{-OH})_4(\text{OH})_4(\text{H}_2\text{O})_4(\text{H}_2\text{tcpp})_2$ | 415 | ~644 | 120 | pH sensing |
| Ag | $\text{riboflavin} @ [\text{AgL}^{25}]_n \cdot n\text{H}_2\text{O}$ | 300 | 537 | 121 | Melamine and acetoguanamine sensing |
| Cd | $\text{Cd}_2(\text{L}^{26})_2(\text{bpa})_2 \cdot 2\text{H}_2\text{O} \cdot 2\text{MeOH}$ | - | - | 122 | Ln encapsulation, tunable emission |
| | $[\text{Cd}_2(\text{tcpe})(\text{DEF})(\text{C}_2\text{H}_5\text{OH})_2] \cdot \text{DEF}$ | 296 | 455 | 51 | Small molecule sensing |
| | $\text{Cd}_2(\text{btc})_2(\text{H}_2\text{O})_2$ | 315 | 406 | 123 | Explosive sensing |
| | $\{(\text{H}_2\text{NMe}_2)[\text{Cd}(\text{taa})]\} \cdot 2\text{H}_2\text{O}$ | 318 | 432 | 124 | PL thermometer |
| | $[\text{Cd}(\text{L}^{27})_2(\text{ClO}_4)_2] \cdot \text{H}_2\text{O}$ | 327 | ~460 | 125 | I ₂ encapsulation and sensing |
| | $[\text{Cd}(\text{ndc})_{0.5}(\text{pca})]$ | 340 | 384 | 66 | Explosive sensing (I) |
| | $[\text{Cd}_3(\text{cpeip})_2(\text{DMF})_3] \cdot \text{DMF} \cdot \text{EtOH} \cdot 2\text{H}_2\text{O}$ | 342 | 392 | 126 | Explosive sensing |
| | $[\text{Cd}_2(\text{L}^{28})(\text{H}_2\text{O})_2] \cdot 6.5\text{DMF} \cdot 3\text{EtOH}$ | 368 | 440 | 127 | Amino alcohol sensing |
| | $[(\text{CH}_3)_2\text{NH}_2]_{15}[\text{Cd}_2\text{Cl}_3(\text{tatpt})_4] \cdot 12\text{DMF} \cdot 18\text{H}_2\text{O}$ | 370 | 425 | 30 | Ir dye doping, white light |
| Cd-Rb | $(\text{Me}_2\text{NH}_2)[\text{RbCd}_4(\text{oba})_5] \cdot \text{H}_2\text{O}$ | 312 | 427, 566 | 128 | Excitation tunable emission, white light |
| In | $[\text{In}(\text{OH})(\text{bdc})]$ | 270 | 326 | 129 | Odorant sensing |
| | $[\text{In}_2\text{L}^{29}][\text{NH}_2(\text{CH}_3)_2] \cdot (\text{DMF})_4(\text{H}_2\text{O})_{16}$ | 280 | 360 | 130 | Explosive sensing (I) |
| | $\text{In}(\text{btb})_{2/3}(\text{oa})(\text{DEF})_{3/2}$ | 380 | 475 | 28 | White light |
| Ln | $\text{LnL}^{30} \cdot \text{DMF}$ | - | - | 131 | Ln doping tunable emission, white light |
| | $[\text{Ln}_2(\text{L}^{31})_2] \cdot (\text{H}_2\text{O})_3 \cdot (\text{Me}_2\text{NH}_2)_2$ | - | - | 132 | Ln doping tunable emission, white light |
| Ln-Na | $[\text{NaLn}(\text{tart})(\text{bibdc})(\text{H}_2\text{O})_2]$ | - | - | 133 | Ln doping tunable emission |
| Ln-Zn | $[\text{H}(\text{H}_2\text{O})_8] \cdot [\text{LnZn}_4(\text{imdc})_4(\text{Him})_4]$ | - | - | 134 | Ln doping tunable emission, white light |
| La | $\text{La}_2(\text{pda})_3(\text{H}_2\text{O})_5$ | 312 | 408 | 135 | Ln doping tunable emission |
| Nd | $[\text{NdCl}(\text{bpdc})(\text{DMF})]$ | 327 | 893, 1060, 1336 | 136 | NIR emission |
| Eu | $[\text{Eu}_2(\text{fma})_2(\text{ox})(\text{H}_2\text{O})_4] \cdot 4\text{H}_2\text{O}$ | 276 | 590, 617, 698 | 75 | Spore sensing |
| | $[\text{Eu}(\text{btc})(\text{H}_2\text{O})] \cdot (\text{H}_2\text{O})_{1.5}$ | 285 | ~620, 700 | 22 | VOC sensing |
| | $[\text{L}^{4+}(\text{bdc})_3 \cdot \text{Eu}_2 \cdot 2\text{H}_2\text{O}]$ | 310 | 590, 614, 651, 687, 697, 700 | 137 | Ln sensing |
| | $\text{Eu}_2(\text{bdc})_3(\text{H}_2\text{O})_2(\text{H}_2\text{O})_2$ | 317NS | 590, 617, 698 | 138 | Nitroaromatic sensing (I) |
| | EuL^{32} | 320 | 579, 591, 611, 650, 698 | 139 | Fe ³⁺ sensing |
| | $\text{Eu}(\text{fbpt})(\text{H}_2\text{O})(\text{DMF})$ | 320 | 590, 616, 651, 698 | 140 | Small molecule sensing, Cu ²⁺ sensing |
| | $[\text{Eu}(\text{pdc})_{1.5}(\text{DMF})] \cdot (\text{DMF})_{0.5}(\text{H}_2\text{O})_{0.5}$ | 321 | ~590, 618, 700 | 22 | Cu ²⁺ sensing |
| | $[\text{Eu}_2(\text{L}^{33})_3(\text{H}_2\text{O})_4] \cdot 3\text{DMF}$ | 323 | 578, 590, 616, 698 | 76 | DMF turn-on |
| | $[\text{Eu}_2(\text{mfda})_2(\text{HCOO})_2(\text{H}_2\text{O})_6]$ | 335 | 580, 592, 614, 618, 651, 700 | 141 | Fe ³⁺ sensing, picric acid sensing |
| | $\text{Eu}_3(\text{mfda})_4(\text{NO}_3)$ | 336 | 581, 592, 615, 620, 654, 703 | 142 | Explosive sensing |
| | $[\text{Eu}(\text{btpeca})(\text{H}_2\text{O})] \cdot n\text{DMF}$ | 344 | 590, 618, 650, 702 | 57 | Cation ²⁺ sensing |
| | Eu-tca | 350 | ~430, 592, 615, 650 | 85 | NO bio sensing |
| | EuL^{34} | 350 | 592, 612, 649, 696 | 143 | Fe ³⁺ sensing |
| | $[\text{Eu}_2(\text{bqdc})_3(\text{H}_2\text{O})(\text{DMF})_3] \cdot 0.5\text{DMF} \cdot \text{H}_2\text{O}$ | 368 | 581, 594, 621, 653, 700 | 144 | Hg ²⁺ sensing |
| | $\{[\text{Eu}(\text{ba})(\text{bpybc})_{1.5}(\text{H}_2\text{O})] \cdot 2\text{NO}_3 \cdot 5\text{H}_2\text{O}\}$ | 465 | 594, 616, 651, 694 | 145 | UV shut-off |
| Eu-Sr | $\infty 3[\text{Sr}_{1-x}\text{Eu}_x(\text{im})_2]$ | 366 | 508 | 146 | Green emission, ~80% quantum efficiency |
| Eu-Ag | $[\text{EuAg}_3(3\text{-tpymntb})_2(\text{H}_2\text{O})(\text{MeCN})](\text{ClO}_4)_6 \cdot 4\text{MeCN}$ | 310 | 510, 579, 592, 614, 649, 695 | 147 | White light |

| | | | | | |
|----------|--|-----|--|---------|--|
| Eu-Ba | $\infty 3[\text{Ba}_{1-x}\text{Eu}_x(\text{im})_2]$ | 365 | 560 | 29 | Yellow light |
| Eu-Tb | $[\text{Eu}_{2x}\text{Tb}_{2(1-x)}(\text{bpd}^*)(\text{bdc})_2(\text{H}_2\text{O})_2]$ | 300 | 487, 544 , 594, 614, 652, 700 | 148 | Small molecule sensing, F ⁻ sensing |
| Eu-Tb-Ni | $[\text{Ni}(\text{L}^{35})\text{Eu}_x\text{Tb}_y(\text{H}_2\text{O})(\text{dmf})_2](\text{NO}_3)_3 \cdot 3\text{H}_2\text{O} \cdot \text{DMF}$ | - | - | 149 | Ln encapsulation, tunable emission |
| Eu-Tb-La | $\text{Ln}_2(\text{L}^{36})_2 \cdot \text{DMF}$ | - | - | 150 | NLO SHG response |
| Eu-Tb-Gd | $[\text{Ln}_7(3,5\text{-dsb})_4(\text{OH})_9(\text{H}_2\text{O})_{15}] \cdot 4\text{H}_2\text{O}$ | - | - | 151 | PL thermometer |
| | $\infty 2[\text{Gd}_{2x}\text{Eu}_x\text{Tb}_y\text{Cl}_6(\text{bipy})_3] \cdot 2\text{bipy}$ | 307 | 488, 546 , 588, 621, 652, 667, 680, 702 | 152 | Ln doping tunable emission, solid solution |
| Tb | $[\text{Tb}(\text{L}^{37})(\text{C}_2\text{H}_2\text{O}_4)_{0.5}(\text{H}_2\text{O})_2] \cdot 2\text{H}_2\text{O}$ | NS | 487, 542 , 581, 620 | 153 | Water sensing |
| | $[\text{Tb}(\text{dpa})(\text{Hdpa})]$ | 294 | ~480, 548 , 582, 620 | 154 | Gunshot residue detection |
| | $[\text{Tb}(\text{fda})_{1.5}]$ | 300 | 488, 543 , 592, 615, 654, 701 | 155 | Small molecule sensing |
| | Tb-tca | 350 | 435, 495, 540 , 582, 615 | 156 | Salicylaldehyde sensing |
| | Tb(btc) | 353 | ~495, 548 , 587 | 22, 157 | F ⁻ sensing, picric acid sensing |
| Tb/Ag | Tb-amp-Ag | 293 | 488, 545 , 584, 620 | 158 | VOC sensing |
| Tb-Cd | $[\text{Cd}_3\text{Tb}_2(\text{btc})_4(\text{H}_2\text{O})_6(\text{DMF})_4]$ | 350 | 490, 544, 584, 620 | 159 | Small molecule sensing, cation sensing |
| | $[\text{Tb}_2(\text{oda})_6\text{Cd}_3(\text{H}_2\text{O})_6] \cdot 6\text{H}_2\text{O}$ | 355 | ~490, 548 , 580, 620 | 69 | Small molecule sensing |
| | $[\text{Cd}(\text{H}_2\text{O})_6] \cdot [\text{Tb}_2(\text{oda})_6\text{Cd}_2] \cdot \text{H}_2\text{O}$ | 378 | ~490, 548 , 580, 620 | 69 | Mn ²⁺ sensing |
| Tb-Eu | $\text{Tb}_{0.9}\text{Eu}_{0.1}(\text{pia})$ | 360 | 491, 546 , 585, 615 | 160 | PL thermometer |
| | $\text{Tb}_{0.99}\text{Eu}_{0.01}(\text{bdc})_{1.5}(\text{H}_2\text{O})_2$ | 320 | ~490, 550, 590, 623 , 650, 700 | 161 | PL thermometer |
| | $\text{Tb}_{0.9931}\text{Eu}_{0.0069}(\text{dmbdc})_3(\text{H}_2\text{O})_4 \cdot \text{DMF} \cdot \text{H}_2\text{O}$ | 381 | ~490, 550, 590, 620 , 652, 701 | 162 | PL thermometer |
| Yb | Yb(bpt) | 326 | 980 | 163 | Small molecule sensing |
| Pb | $[\text{Pb}_3(\text{bpt})_2-(\text{phen})_2] \cdot \text{phen}$ | 390 | 455 , 575 | 164 | Excitation tunable yellow/violet dual emission |
| Bi-Cd | $\text{Bi}_2\text{Cd}(2,6\text{-pdc})_4(\text{H}_2\text{O})_2 \cdot \text{H}_2\text{O}$ | 324 | 441, 470 | 165 | Ln doping tunable emission, white light |

Metals separated by a (-) indicates heterometallic PBU or SBUs, where a (/) indicates that the second metal is part of the ligand. Names for the ligands (Lⁿ) can be found in the list of abbreviations at the end of the review. NS = excitation wavelength not explicitly stated; **bold** = emission maximum; *italicized* = broad emission (FWHM >100 nm).

In order to fully explore the virtues of LMOFs as sensory materials, rational design, control, and construction of their structures become a necessity. The existing gas and hydrocarbon adsorption studies are among the most valuable assets for MOF based applications, and have profound significance in designing sensors with superb performance. When screening existing LMOFs as potential sensors, priority should be given to those that selectively adsorb targeted analytes. Precision for the adsorption of an analyte molecule is usually achieved through the accurate construction of a desired pore on the molecular level.^{22, 166} Size exclusivity is the most intuitive selection rule, where only molecules slimmer than the pore can be captured. Thus, controlling the pore size is seemingly the most obvious first step to consider when designing LMOF based sensors. The porosity of MOFs provides such a versatile platform to work with, and is subject to various chemical manipulations. Many physicochemical properties within the porous environment, such as hydrophobicity, polarity, polarizability, acidity and proton affinity, can be finely-tuned. By controlling the chemical environment of the pore, selective capture of targeted molecules can often be achieved. For instance, the incorporation of Lewis basic site (LBS) facilitates the attraction of metal ions¹⁶⁷ and the acidic 2,4,6-trinitrophenol (TNP)¹⁶⁶. Earlier study also demonstrated the utilization of open metal site (OMS) for sensing small molecules.¹⁶⁸ In a recent case, the effective detection of NH₃ is realized by the preferential binding of this guest molecule at an OMS.⁷⁴ In another case, anion recognition is attained through the hydrogen bonding between analyte and terminal solvent molecule.¹⁶⁹ The electronic properties of LMOFs are also crucial with respect to their sensing behaviors. Electron and/or energy transfer between an LMOF and an analyte are the main reasons for a fluorescent response, and as such, rational design of a LMOF should aim at promoting these features. The introduction of highly conjugated linkers in a framework is expected to better attract aromatic or conjugated analytes through π - π interactions.⁹⁴ The relative orbital energies of the CB (or LUMO) of LMOFs can be tailored by incorporating electron-donating or electron

withdrawing groups into the ligands.¹⁷⁰ In terms of energy transfer, it has been demonstrated that the overlap between the emission spectrum of an LMOF and the absorption spectrum of a specific analyte induces a dramatic decrease in the fluorescence intensity of the LMOF.⁶⁶ The real-world use of LMOF sensors demands superb sensitivity and selectivity. As more and more LMOF sensors are being discovered, it is foreseeable that precise identification of a targeted analyte may eventually become possible by a cross-referencing method employing a series of LMOFs selected from a large library of sensory materials.

2. Luminescence Based Sensing Applications

LMOFs have been widely explored in many sensory applications due to their unique ability to selectively capture analyte molecules. Their permanent porosity often serves as a powerful platform for the reversible adsorption and release of these molecules. Therefore, LMOF based sensors can be highly recyclable and economically effective. LMOFs have been proven successful in the detection of volatile organic compounds, small molecules, and ionic species. The thermochromic properties of some LMOFs have led to the discovery of luminescent thermometers. In addition, the versatile functionalities of LMOFs make them extremely useful in the biological realm, exemplified by bio-sensing and bio-imaging. Another sphere of luminescence based sensing application is the detection of energetic materials, such as explosives and explosive-like molecules, which will be discussed thoroughly in Section 3.

2.1 Sensing of Volatile Organic Compounds and Small Molecules

Dincă and coworkers recently explored a new territory of sensing volatile organic compounds (VOCs) at elevated temperatures.⁷⁴ Two LMOFs, Zn₂(tcpe) and Mg(dhbc) (tcpe = tetrakis(4-carboxyphenyl)ethylene; dhbc = 2,5-

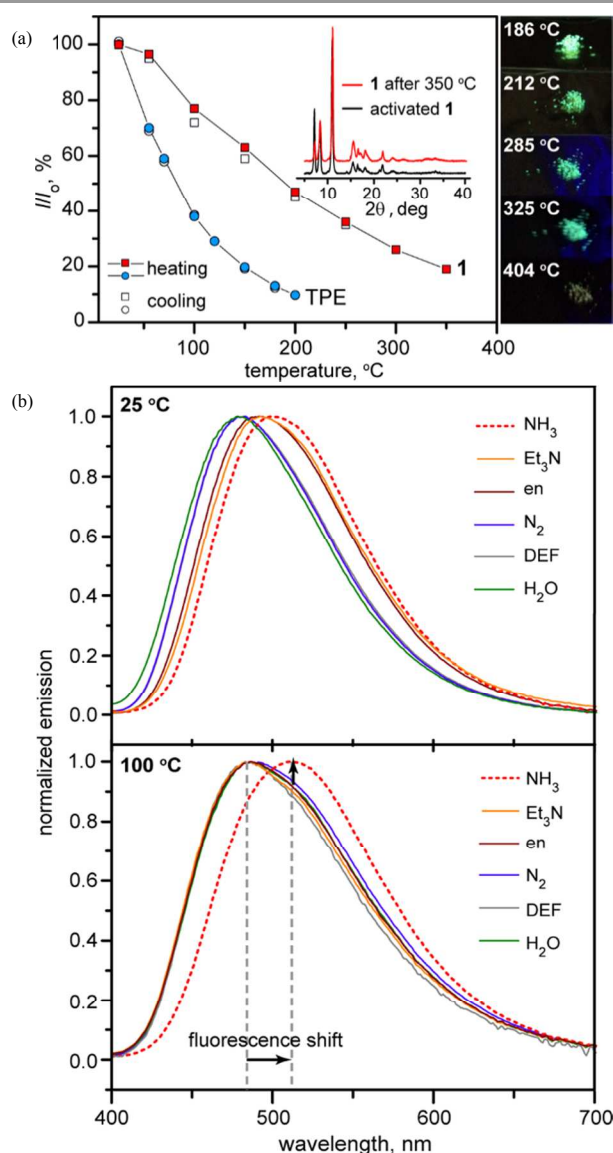


Figure 1. (a) Fluorescence decay of $Zn_2(tcpe)$ (squares) and tpe (tetraphenylethylene) (circles) with increasing temperature. PXRD patterns of $Zn_2(tcpe)$: activated and after heating are inserted. The optical images show the fluorescence of $Zn_2(tcpe)$ ($\lambda_{ex} = 350$ nm) at different temperatures in air. (b) Emission spectra of $Zn_2(tcpe)$ ($\lambda_{ex} = 350$ nm) after exposure to analytes at 25 and 100 °C. Reprinted with permission from Ref 74. Copyright 2013 American Chemical Society.

dihydroxybenzene-1,4-dicarboxylate), were chosen for this study, both of which maintain their strong fluorescence at relatively high temperatures.^{51, 82} For $Zn_2(tcpe)$, exposure to a series of analytes (NH_3 , triethylamine (Et_3N), ethylenediamine (en), N_2 , N,N -diethylformamide (DEF), and H_2O) at room temperature shifts the emission maximum to various extents. Interestingly, the selectivity of this LMOF is switched on at high temperature. At 100 °C this material exhibits remarkable selectivity for NH_3 when all the other analytes are silenced: only NH_3 is able to shift the emission wavelength maximum by 24 nm, as shown in Figure 1. Computational study revealed that NH_3 has strong binding affinity to the open metal sites within the MOF framework which may be responsible for the

temperature dependent emission frequency shift. For $Mg(dhbc)$, while ammonia and methanol have similar binding energies, the smaller kinetic diameter of ammonia makes it more accessible to the small pores of this LMOF, while methanol is excluded due to its larger kinetic diameter, hence its emission frequency shift does not change as a function of temperature. The authors demonstrated a successful attempt at combining molecular sieving and chemical selectivity for the detection of a targeted molecule. The retention of an LMOF's fluorescence at higher temperatures is rarely replicable in organic conjugate polymers; this unique property can be of great assistance in studying the photophysics of fluorescent materials at non-ambient conditions.

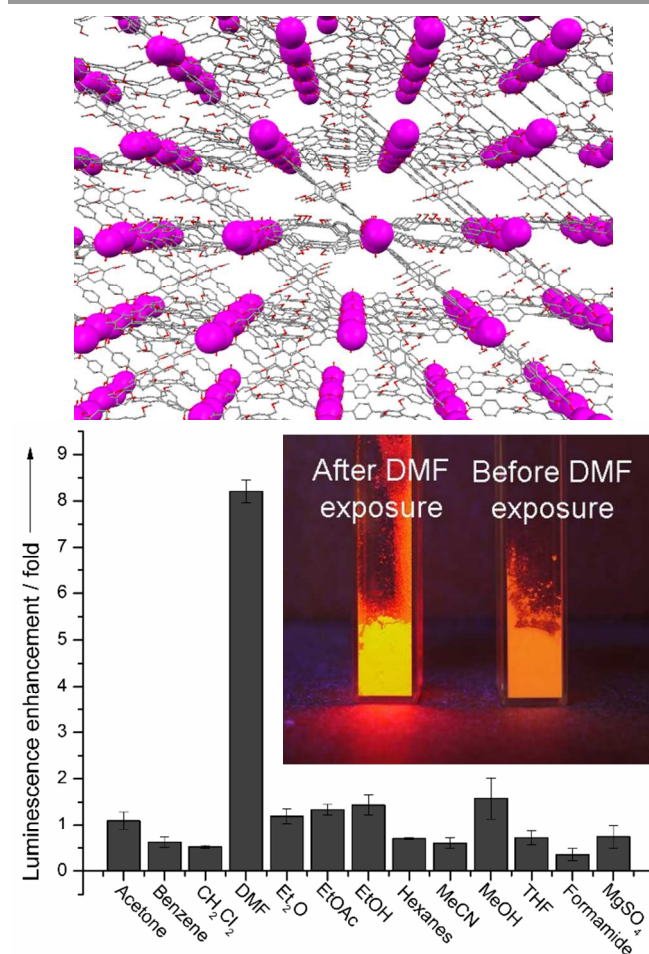


Figure 2. Top: The overall 3D structure of $[Eu_2(L^{33})(H_2O)_4] \cdot 3DMF$ with open channels. (Hydrogen atoms and solvent molecules are removed.) Bottom: The fluorescence enhancement of the water-exchanged Eu-MOF after exposure to analytes. The insert is an image of the Eu-MOF at “on” and “off” stages under UV excitation. Adapted with permission from Ref 76. Copyright 2013 Wiley-VCH.

In another case, “turn-on” detection for N,N -dimethylformamide (DMF) in the vapor phase was demonstrated by Li and coworkers (Figure 2).⁷⁶ The detection of DMF is of great importance since both human and animal experiments suggested that DMF is associated with serious health issues due to its hepatotoxicity.^{171, 172} A lanthanide

LMOF, $[\text{Eu}_2(\text{L}^{33})_3(\text{H}_2\text{O})_4]\cdot 3\text{DMF}$ ($\text{L}^{33} = 2',5'$ -bis(methoxymethyl)-[1,1':4',1''-terphenyl]-4,4''-dicarboxylate)), was activated by soaking in water for three days. The emission intensity of the water-exchanged framework was enhanced upon exposure to various solvent vapors, among which DMF triggers the most significant “turn-on”: more than an eightfold enhancement of the emission intensity was demonstrated, as seen in Figure 2d. A fluorescence lifetime study on water exchanged and deuterated water exchanged LMOF samples implied that the removal of water from the Eu centers contributes greatly to the enhanced fluorescence since water quenches the Eu centered emission. But more importantly, the adsorption of DMF into the porous structure not only constrains the free rotation of phenyl rings present in the linker ligand, but also perturbs the energy levels of the linker, which results in a favorable LMCT process and thus strongly enhances the emission of the sensor. The authors also took a further step in testing the response rate of the sensor: 95% of “turn-on” can be achieved within a few minutes. This sensor can be conveniently recycled by purging with water vapor for a few seconds.

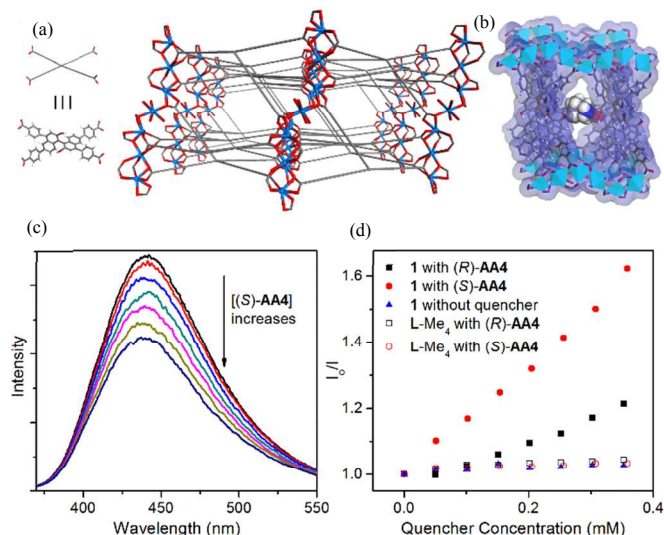


Figure 3. (a) Ball-and-stick representation of the structure of $[\text{Cd}_2(\text{L}^{28})(\text{H}_2\text{O})_2]\cdot 6.5\text{DMF}\cdot 3\text{EtOH}$ viewed along the [010] direction. (b) Amino alcohol inside a LMOF channel. (c) Fluorescence emission of $[\text{Cd}_2(\text{L}^{28})(\text{H}_2\text{O})_2]\cdot 6.5\text{DMF}\cdot 3\text{EtOH}$ with the incremental addition of an amino alcohol. (d) Stern-Volmer plots of the fluorescence of the LMOF and a molecular analogy of the linker, quenched by the enantiomers of an amino alcohol. Adapted with permission from Ref¹²⁷. Copyright 2012. American Chemical Society.

With precise control of the pore morphology and the chemical environment within the cavity, not only can molecules with different compositions be differentiated, the chemoselectivity can also be raised to a higher level, that is, the recognition of stereoisomers. Lin et al. designed an enantioselective sensor based on a 1,1'-bi-2-naphthol (BINOL) derivative.¹²⁷ BINOL derivatives have been explored as fluorescent enantiomer sensors for a diverse group of chiral compounds that are subject to the formation of hydrogen bonds

with the hydroxyl groups on the BINOL's core. Immobilization of this functional moiety into a rigid porous structure has an obvious advantage: the confinement of analyte molecules in the cavities preconcentrates and places the analyte in close proximity to the functional sites of the framework, where an analyte-functional site interaction may lead to enhanced sensitivity. With this inspiration, $[\text{Cd}_2(\text{L}^{28})(\text{H}_2\text{O})_2]\cdot 6.5\text{DMF}\cdot 3\text{EtOH}$ ($\text{L} = (\text{R})$ -2,2'-dihydroxy-1,1'-binaphthyl-4,4',6,6'-tetrakis(4-benzoic acid)) was synthesized for detecting the enantiomers of amino alcohols. This LMOF responds to amino alcohols in the form of fluorescence quenching, possibly through the formation of hydrogen bonds between the analytes and ground state BINOL moieties, and the subsequent occurrence of a low emissive excited state charge-transfer via the assistance of proton-transfer. As expected, this LMOF shows superior sensitivity for amino alcohols compared to previously reported homogeneous BINOL-based sensors. The preconcentration effect was confirmed by gas chromatography (GC), as the concentration of the studied amino alcohol within the pores of the LMOF is a few thousand times higher than in the supernatant. These findings led to the postulation that these quencher molecules are better accommodated within the LMOF cavities than in the solvent used to disperse the LMOF particles. Among all of the tested amino alcohols, this sensor shows superb selectivity towards the enantiomers of 2-amino-3-methyl-1-butanol. Furthermore, the quenching response correlates well with the enantiomeric excess (ee) of 2-amino-3-methyl-1-butanol. Therefore, this LMOF sensor can easily determine the ee of amino alcohol samples by a rapid fluorescence quenching titration (see Figure 3). The amplified chiral selectivity in this porous LMOF can be utilized in the design of other LMOF sensors.

Other VOCs and small molecules, such as H_2S , H_2O , CO_2 , and common solvent molecules, are also successfully detected by LMOFs. The Ag^+ functionalized Tb-amp (amp = adenosine monophosphate) responds to H_2S via fluorescence quenching achieved by the formation of Ag_2S .¹⁵⁸ The PL intensity of the 2D LMOF $\text{MV}[\text{Mn}_2\text{Cu}_3(\text{mpba})_3(\text{H}_2\text{O})_3]\cdot 20\text{H}_2\text{O}$ increases with incremental water loading, and its emission shifts upon exposure to CO_2 .⁸⁷ The solvatochromic property of $[(\text{CuCN})_3\text{L}^1(\text{guest})_x]_n$ enables it to differentiate solvents as the emission frequency shifts upon exposure to various solvents. More interestingly, the vapor of acetonitrile induces the time-dependent fluorescence enhancement which can be used to monitor this analyte.⁸⁴

2.2 Sensing of Ionic Species

Colorimetric detection is probably the most desired method among sensing mechanisms simply because its visible signal transduction does not require the assistance of any additional instrumentation. Xu et al. exemplified colorimetric detection of the noble metal cation Pd (II) with ASMOF-5, an LMOF isorecticular to the prototypical MOF-5, but constructed from Zn^{2+} and 2,5-dithioaloxysterphthalic acid.⁵⁵ The sulfur-conjugated aromatic core is responsible for the fluorescence of this compound, and the thioether moiety strongly attracts the

noble-metal ion. In addition, the alkene side chain provides additional affinity to the noble-metal species. Upon exposure to Pd^{2+} in solution at a ppm level concentration, ASMOF-5 changes from light yellow to orange-red as shown in Figure 4b. Other metal ions do not affect the color of the crystal at low concentrations (5 ppm), and turn the color of the crystal to brownish grey (or green for Cu^{2+}) at high concentrations (1500 ppm). The unique color caused by Pd^{2+} is easily distinguished from the less characteristic color change caused by other metal ions. By combining thioether and alkene moieties, ASMOF-5 turns out to be an excellent colorimetric sensor for Pd (II) species.

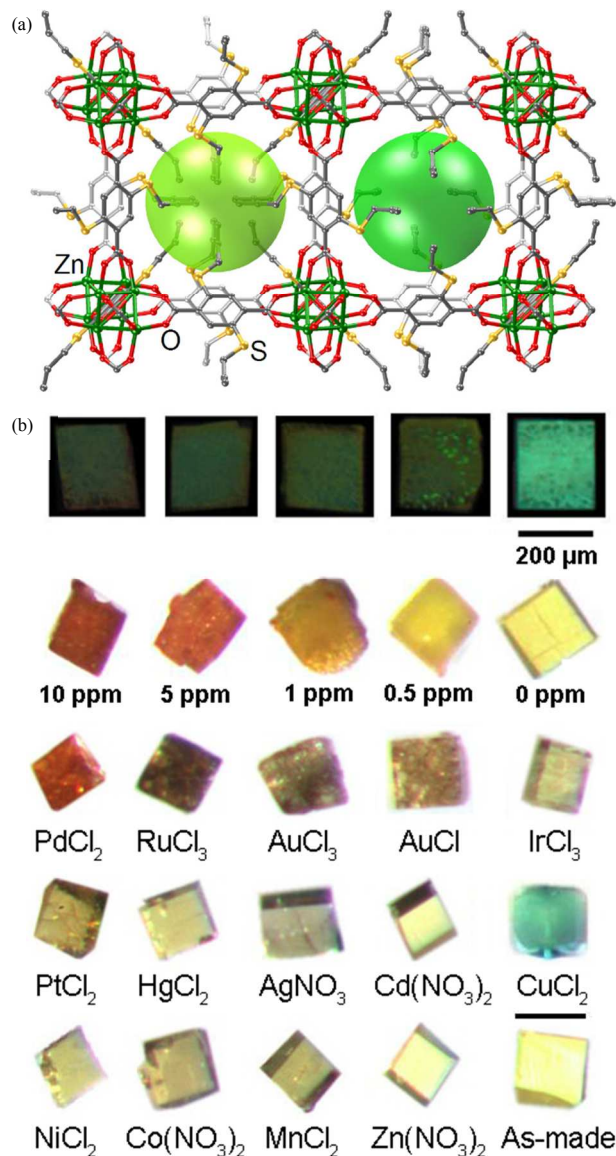


Figure 4. (a) An illustration of the cavities in ASMOF-5. (b) Photographs of ASMOF-5 crystals after exposure to Pd (II) of various concentrations at 80 °C, under UV (365nm, top row) and ambient light (bottom row). (c) Photographs of ASMOF-5 crystals after exposure to different metal ions under ambient light. The black bar indicates 200 μm . Reprinted with permission from Ref 55. Copyright 2013 American Chemical Society.

In the design and screening of functional LMOFs for sensing applications, the stability is an important factor to consider. A large number of MOFs are thermally robust as they can stand heating in a protected environment to a few hundred degrees Celsius. But the vast majority of reported MOFs are sensitive to water or moisture, which limits their applications in humid or aqueous environments. Guided by soft/hard acid-base theory,

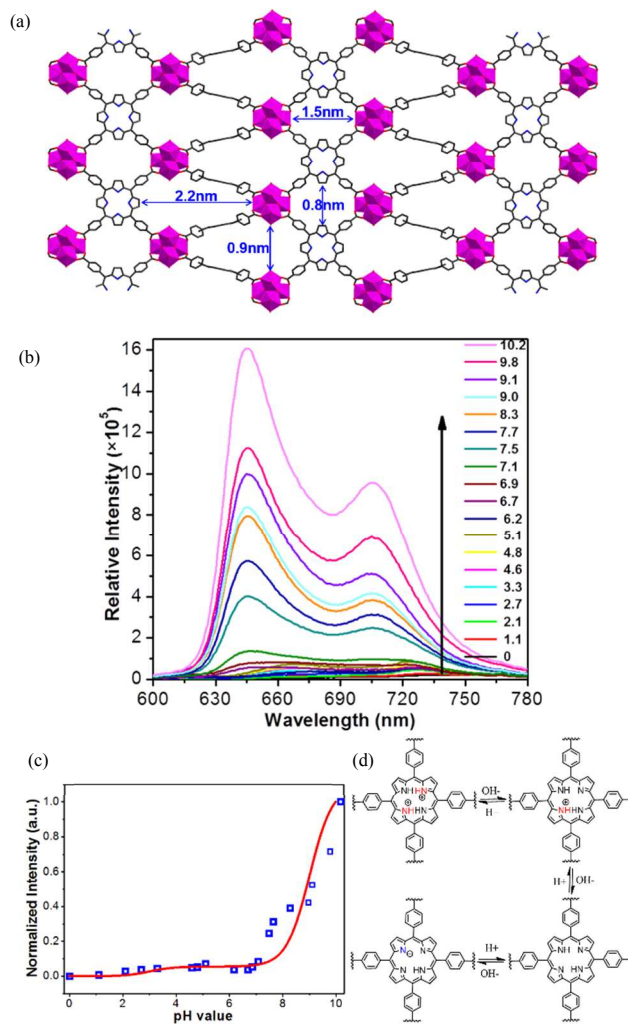


Figure 5. (a) View along the b-axis of PCN-225 showing two types of channels. (b) The fluorescence spectra of PCN-225 under different pH values ($\lambda_{\text{ex}} = 415 \text{ nm}$). (c) Experimental (blue square) and simulated (red line) pH-dependent fluorescence. (d) An illustration of protonation and deprotonation of porphyrin core. Adapted with permission from Ref 120. Copyright 2013 American Chemical Society.

Zhou and coworkers have demonstrated that by forming a strong metal-oxygen bond between the zirconium (IV) cation (hard acid) and a carboxylate anion (hard base), a series of thermally and chemically stable porous compounds can be realized.^{120, 173, 174} Their recent work highlighted a Zr based porphyrinic LMOF with exceptional thermal stability ($\geq 350 \text{ }^\circ\text{C}$) and high resistance to changes in pH (1 to 11) in aqueous media.¹²⁰ The combination of stability under a wide range of pH values and the dye characteristics of the porphyrin centers

led to PCN-225, a fluorescent pH indicator as shown in Figure 5. The pH-dependent fluorescence originates from the protonation or deprotonation of the porphyrin core. Under acidic conditions (pH < 5) the protons on the pyrrole rings stay intact, while the pyridine-type nitrogen atoms gradually get protonated with increasing acidity. This protonation disharmonizes the conjugated π -electron system of the porphyrin ring and therefore leads to quenched fluorescence. Under basic conditions, the deprotonation of the imino groups are held responsible for the

of Eu^{3+} .¹⁰⁴ In addition, Liu et al. found that the PL intensity and quantum efficiency of $[\text{Cd}(\text{H}_2\text{O})_6][\text{Tb}_2(\text{oda})_6\text{Cd}_2]\cdot\text{H}_2\text{O}$ decreases with increasing Mn^{2+} content. Liu, Zheng et al. reported Fe^{3+} sensing using $[\text{Eu}(\text{btpca})(\text{H}_2\text{O})]\cdot n\text{DMF}$.⁵⁷ In the case of anion detection, Ghosh and coworkers utilized the cationic framework $[\text{Zn}(\text{L}^{18})(\text{H}_2\text{O})_2](\text{NO}_3)_2\cdot 2\text{H}_2\text{O}$ and exchanged the nitrate counter-anion with anionic species such as ClO_4^- , $\text{N}(\text{CN})_2^-$, N_3^- , and SCN^- to achieve tunable emission.⁵⁶

2.3 Biosensing and Biomedical Imaging

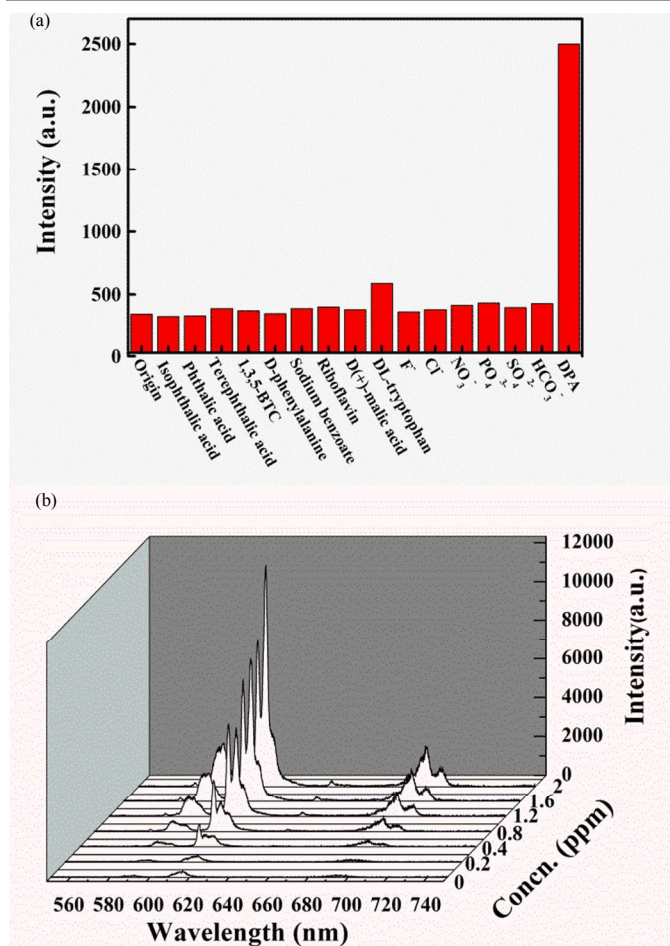


Figure 6. (a) Fluorescence intensities of a nanoscale $\text{Eu}_2(\text{fma})_2(\text{ox})(\text{H}_2\text{O})_4\cdot 4\text{H}_2\text{O}$ sample with the addition of 1 ppm of various analytes ($^5\text{D}_0 \rightarrow ^7\text{F}_2$ transition, $\lambda_{\text{ex}} = 279$ nm) in ethanol solution. (b) The emission spectra of the nanoscale Eu-MOF in ethanol with the addition of DPA of different concentrations. Reprinted from Ref 75 with permission. Copyright 2012. The Royal Society of Chemistry.

enhancement in fluorescence. The authors concluded that the change in fluorescence intensity is especially sharp within the pH range of 7 to 10 (Figure 5c), thus PCN-225 is very efficient for pH sensing in this range.

George, Maji, and coworkers reported the sensing of metal ions with $\text{Mg}(\text{dhdcb})$, whose fluorescence is more significantly quenched by Cu^{2+} compared to Ni^{2+} and Co^{2+} .⁶⁸ Li, Su, and coworkers demonstrated the sensing of Eu^{3+} through fluorescence enhancement with $[\text{Zn}_2(\text{L}^{14})(\text{H}_2\text{O})](\text{NO}_3)_2\cdot \text{DMF}$: the emission intensity increases with the incremental addition

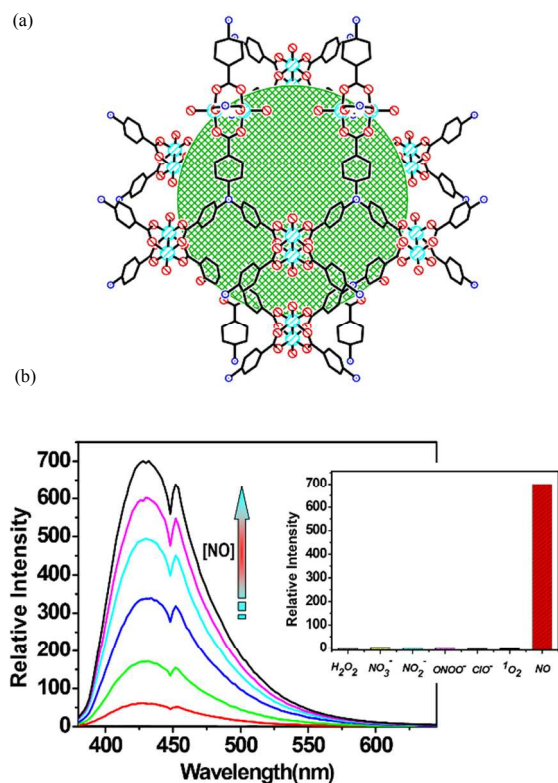


Figure 7. (a) A fragment of Cu-tca showcasing the porous nature and metal coordination of this material. (b) The PL spectra of Cu-tca in a buffer system with increasing NO concentration. The insert shows the emission intensity of Cu-tca after exposure to various reactive oxygen and nitrogen species in buffer. Adapted with permission from Ref 85. Copyright 2012 Wiley-VCH.

As mentioned previously, luminescence sensing may prove to be an effective method for identifying chemically hazardous species. Additionally, it may be efficient for detecting molecules with significant biological implications. Dipicolinic acid (DPA) is one example of such a molecule, as it widely exists in bacterial endospores. Detection of DPA contributes to the prevention of *Bacillus anthracis* related biological attacks.¹⁷⁵⁻¹⁷⁸ Recently, Chen and Qian et al. utilized a nanoscale LMOF, $\text{Eu}_2(\text{fma})_2(\text{ox})(\text{H}_2\text{O})_4\cdot 4\text{H}_2\text{O}$, for the effective turn-on detection of DPA.⁷⁵ Particle size and morphology control of this LMOF¹⁷⁹ were realized by a surfactant-assisted synthetic method. Decreasing the material's particle size to the nanoscale not only ensures uniform dispersion into the solvent,

but also enhances the sensitivity for the detection of DPA. The addition of a small amount of DPA to the LMOF suspension significantly increases the luminescent intensity of the mixture. When the concentration of DPA is 2 ppm, this enhancement can be as high as 90 times that of its original emission intensity. Exposures to the other components that co-exist within the bacterial endospores barely affect the emission intensity of this LMOF, as shown in Figure 6a. Such sensitivity for DPA is likely due to the preferential binding of DPA at the Eu^{3+} center, which can largely facilitate the intramolecular energy transfer.

Besides the indirect approach, directly targeting biomolecules, such as antibodies or molecules involved in

NO led to a 700-fold increase in the fluorescence intensity. It is also worth mentioning that the NO recognition of this LMOF is very specific, as exposure to other possible competitive reactive oxygen and nitrogen species at much higher concentrations does not significantly affect the emission of the sensor. The fluorescence enhancement can be possibly attributed to the reduction of Cu(II) to diamagnetic Cu(I) through a reaction with NO. The formation of Cu(I) then recovers the fluorescence quenched by the paramagnetic Cu(II). The nanoparticles of Cu-tca were obtained by microwave assisted synthesis, and tested successfully in the fluorescent visualization of the NO activity in MCF-7 cells.

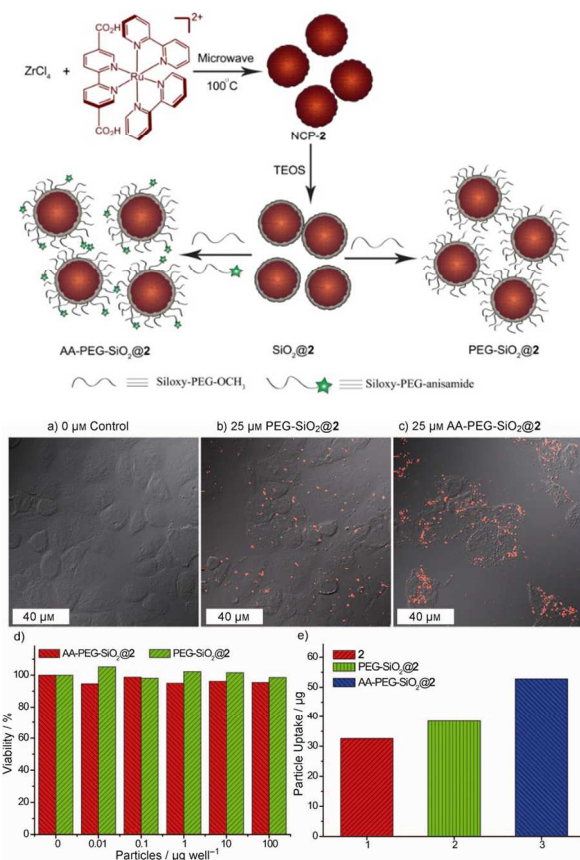


Figure 8. Top: A schematic illustration of the synthesis and functionalization of NCP-2. (a) to (c), Visualization of H460 cells incubated with different amount (type) of particles using confocal microscopy. (d) Viability assay for H460 cells in vitro. (e) Study of particle uptake in H460 cells. Reprinted with permission from Ref 115. Copyright 2011 Wiley-VCH.

biological processes, has also proven feasible with LMOF based biosensors.^{85, 180} Nitric oxide (NO) is one of the key molecules in mediating mammalian functions,¹⁸¹ and as such monitoring NO in biological systems is of great importance. Duan and coworkers demonstrated the luminescent detection of NO under biological conditions with Cu-tca (H_3tca = tricarboxytriphenyl amine), shown in Figure 7.⁸⁵ The Cu-MOF itself has a weak blue emission when excited at 350 nm, possibly due to the quenching effect of the paramagnetic Cu^{2+} . Introduction of NO to the Cu-tca in aqueous solution at room temperature triggered a significant increase in the LMOF's emission: 1 mM

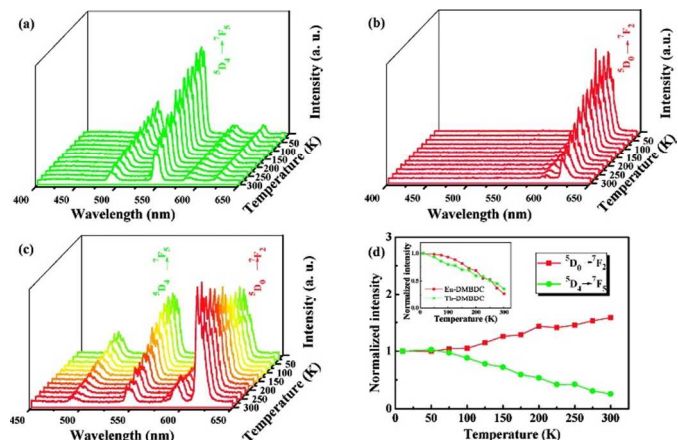


Figure 9. PL emission between 10 and 300 K ($\lambda_{\text{ex}} = 355$ nm) for (a) Tb-dmbdc, (b) Eu-dmbdc, (c) $\text{Eu}_{0.0069}\text{Tb}_{0.9931}$ -dmbdc. (d) Temperature-dependent PL intensities from different transitions for $\text{Eu}_{0.0069}\text{Tb}_{0.9931}$ -dmbdc. Inset figure shows temperature-dependent PL intensities from different transitions for Tb-dmbdc and Eu-dmbdc. Reprinted with permission from Ref 162. Copyright 2012 American Chemical Society.

The structural and chemical diversity of MOFs makes it a class of versatile materials. Seeking to take advantage of their permanent porosity and intrinsic biodegradability, MOFs are also being explored for biomedical imaging either by loading imaging contrast agents into the pore space, or by incorporating luminescent building blocks into the framework.³⁸ Lin and coworkers incorporated a phosphorescent ruthenium complex into Zn^{2+} and Zr^{4+} based frameworks, respectively.¹¹⁵ They employed microwave assisted synthesis to obtain two nanoscale coordination polymers (NCPs). The silica coated Zr based NCP-2 was further functionalized through a surface modification with PEG, a hydrophilic polymer. Uptake studies and confocal microscopy of H460 lung cancer cells in vitro confirmed that the anisamide-PEG (AA-PEG) functionalized compound acts as an efficient optical imaging contrast agent for targeting cancer cells, as shown in Figure 8c.

2.4 Luminescent Thermometers

The optical properties of LMOFs are often affected by temperature. For example, fluorescence intensity typically decreases as the temperature increases, as shown in the case of $\text{Zn}_2(\text{tcpu})$.⁷⁴ Another representative example is $[\text{Zn}_3(\text{tdpat})(\text{H}_2\text{O})_3]\cdot\text{G}$ (G = guest solvent), which shows a linear

decrease in emission intensity with respect to increasing temperature.¹⁰⁷ Temperature-dependent quantum yields have been reported for $\{(H_2NMe_2)[Cd(ttaa)]\} \cdot 2H_2O$ and $\{(H_2NMe_2)[Cd(ttaa)]\} \cdot H_2O$.¹²⁴ As one may expect, these findings give rise to the concept of LMOF based luminescent thermometers. LMOF thermometers can be superior to other conventional thermometers because of their rapid response time, high sensitivity, and strong resistance to electric or magnetic fields.¹⁶²

Qian, Chen and coworkers have developed a mixed-lanthanide LMOF system that shows unique temperature-dependent luminescence behavior, highlighting their potential use as luminescent thermometers.^{151, 160, 162} The two

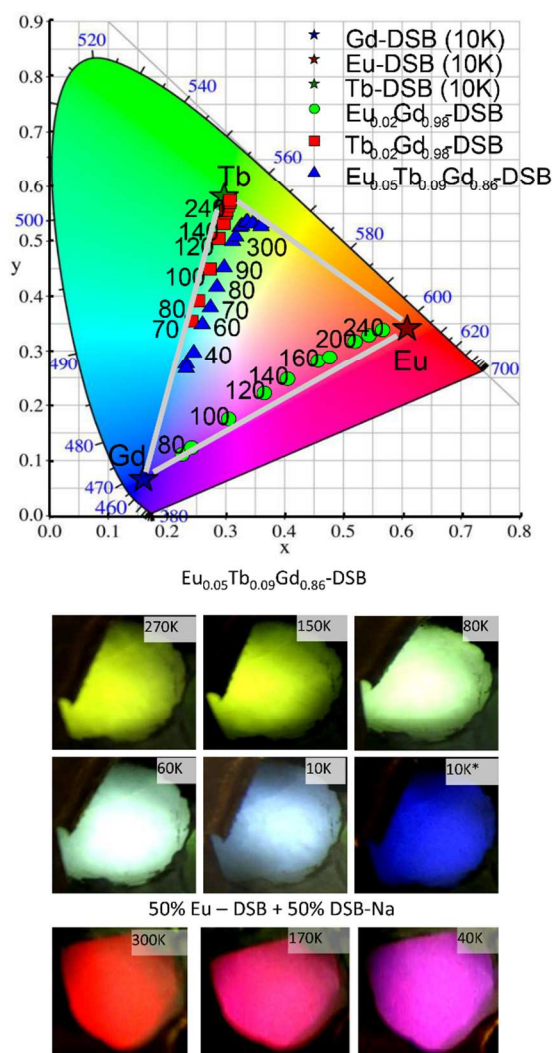


Figure 10. Top: CIE coordinates for $Eu_{0.02}Gd_{0.98}$ -dsb, $Tb_{0.02}Gd_{0.98}$ -dsb and $Eu_{0.05}Tb_{0.09}Gd_{0.86}$ -dsb showing the temperature-dependent emission. Bottom: Photos of the LMOF pellets at various temperatures. (* denotes a triplet emission) Reproduced from Ref 151 with permission. Copyright 2013. The Royal Society of Chemistry.

isostructural 3D MOFs, Tb-dmbdc and Eu-dmbdc (dmbdc = 2,5-dimethoxy-1,4-benzene dicarboxylate), exhibit characteristic lanthanide fluorescence, indicating the strong

sensitizing ability of dmbdc and its effective use as an excellent antenna chromophore. A series of mixed lanthanide LMOFs, Eu_xTb_{1-x} -dmbdc ($x = 0.0011, 0.0046$ and 0.0069), were acquired by varying the molar ratios of the metal salts using the same synthetic method as used for the parent compounds. The resulting mixed lanthanide LMOFs are also isostructural to the parent structures. Besides being sensitized by the ligand, Eu^{3+} ions are also sensitized by Tb^{3+} ions in the mixed lanthanide LMOFs. The metal centered emissions in Eu-dmbdc and Tb-dmbdc gradually decrease with increasing temperature, possibly due to thermally activated nonradiative-decay pathways, as shown in Figure 9a and 9b. Interestingly, the mixed lanthanide MOF $Eu_{0.0069}Tb_{0.9931}$ -dmbdc behaves differently from its parent compound; the Tb^{3+} centered emission decreases while the Eu^{3+} centered fluorescence increases upon heating (Figures 9c and 9d). These different temperature-dependent metal-centered emission behaviors within the same compound enable self-calibration and self-referencing, making the material an ideal candidate for a fluorescent thermometer. Additionally, the emission intensity ratio, I_{Tb}/I_{Eu} , is linearly related to temperature from 50 to 200 K. This unique behavior in the mixed lanthanide LMOF suggests an enhanced energy transfer from Tb^{3+} to Eu^{3+} with increasing temperature. Utilizing the same strategy, Eu_xTb_{1-x} -pia compounds (pia = 5-(pyridin-4-yl)isophthalic acid; $x = 0.01, 0.05, 0.10, 0.20, 0.50$ and 0.80) were also evaluated as fluorescent thermometers and were found to have a sensitivity of 3.53% per K when $x = 0.01$.¹⁶⁰

D'Vries and coworkers further took advantage of the phosphorescence of a ligand, dsb (3, 5-disulfobenzoic acid) in the construction of mixed lanthanide LMOFs: $[Ln_7(3,5-dsb)_4(OH)_9(H_2O)_{15}] \cdot 4H_2O$ ($Ln = Eu, Tb$ and Gd). The rational combination of the three basic colors, blue emission from the ligand, red emission from Eu-dsb, and green emission from Tb-dsb, made possible the functional design of a colorimetric fluorescent thermometer (Figure 10).¹⁵¹ Surfactant and microwave assisted synthesis also enabled the production of LMOF nanoparticles; it is anticipated that the fabrication of fluorescent nanothermometers has great potential for applications in thermal sensing and intracellular activity mapping with nanoscale resolutions.¹⁶²

3. Detection of Explosive and Explosive-like Molecules

3.1 Background

Using LMOF sensors for the detection of high explosives is possibly one of their most promising applications. Detection of these life-threatening energetic materials plays a crucial role in anti-terrorism operations, homeland security, and civilian safety, and thus has the ability to directly save human lives and protect the environment. The continuing rise of terrorist activities around the globe calls for further attention towards developing sensitive and efficient explosive detection methods. Current detection methods employ trained canines (sniffer dogs)¹⁸² in

addition to modern analytical instruments, such as ion mobility spectrometry (IMS),¹⁸³ plasma desorption mass spectrometry (PDMS),¹⁸⁴ surface-enhanced Raman spectroscopy (SERS),¹⁸⁵ energy dispersive X-ray diffraction (EDXRD),¹⁸⁶ and various imaging technologies.¹⁸⁷ These detection methods provide high sensitivity and accuracy, however they suffer from a number of disadvantages, most notably high cost and lack of portability.

Optical sensing has emerged as a new approach that is cost effective, fast, and easily portable. Utilizing the optical properties of fluorescent materials, effective detection of many high explosive or explosive-like molecules can be achieved.¹⁸⁸ Organic conjugate polymers represent a group of such materials that have bloomed over the past decade.^{61, 67, 189} Portable devices based on amplifying fluorescent polymers (AFPs) have been made available, and explosive sniffing robots have been utilized for military ventures for quite a few years.¹⁹⁰ With that said, the stage is now set for LMOF sensing to shine. As mentioned throughout this review, the permanent porosity and electronic tunability of these materials, coupled with rational design and engineering of their crystal and pore structures, allow one to finely tune the chemical environment within and on the surface of the framework. A meticulously designed LMOF may then facilitate the pre-concentration and recognition of a targeted analyte, leading to superior sensitivity and selectivity. These features highlight LMOFs as amazing candidates for the detection of explosives.

As a category, "explosive and explosive-like molecules" encompasses a diverse group of compounds, as illustrated in Figure 11. Accurate recognition of an analyte molecule relies on a sensory material's ability to specifically interact with the targeted species. For example, TNT is subject to the formation of a Meisenheimer complex with certain nucleophiles.^{191, 192} A dual emission hybrid material, comprised of quantum dots with

polyamine functionalized surfaces, was designed to exploit this property of TNT and instant visual detection was achieved.¹⁹³ The photolytic cleavage of nitroesters and nitramines was utilized in the selective "turn-on" detection of PETN and RDX.¹⁹⁴⁻¹⁹⁶ Furthermore, the photo-induced oxidation of the fluorene moiety by nitrate esters was employed by a polymeric fluorescent sensor to generate a selective "turn-on" response from TNG and PETN.¹⁹⁷ These strategies are also applicable with regards to LMOF based sensors. Incorporation of the aforementioned functional moieties into porous frameworks is worth exploring for the accurate recognition of desired analytes via the chemical approach, where the analytes chemically react or interact with the sensory materials. In addition, the permanent porosity of many LMOFs adds another dimension for molecular recognition through size exclusion.

Understanding the physicochemical nature of a given analyte molecule is of absolute necessity for the design of an effective sensor. For example, the LUMO energy of an analyte is an important factor to consider: its relative level to the LUMO (or conduction band, CB) of a sensor material, determines the direction of electron transfer upon photoexcitation. This is especially useful in predicting and understanding the form of the fluorescence response, whether it be enhancement or quenching.^{62, 73}

Quantitative evaluation of the quenching efficiency of a particular sensor can be achieved using Stern-Volmer analysis (Equation 1).^{197, 198} In this formula I_0 is the fluorescent intensity of the sensory material before the addition of the quencher, I_f is the intensity after the quencher is added, and k_{sv} is the Stern-Volmer constant, where high a k_{sv} value is usually associated with efficient sensors.

$$I_0/I_f = 1 + k_{sv} \cdot [Q] \quad (1)$$

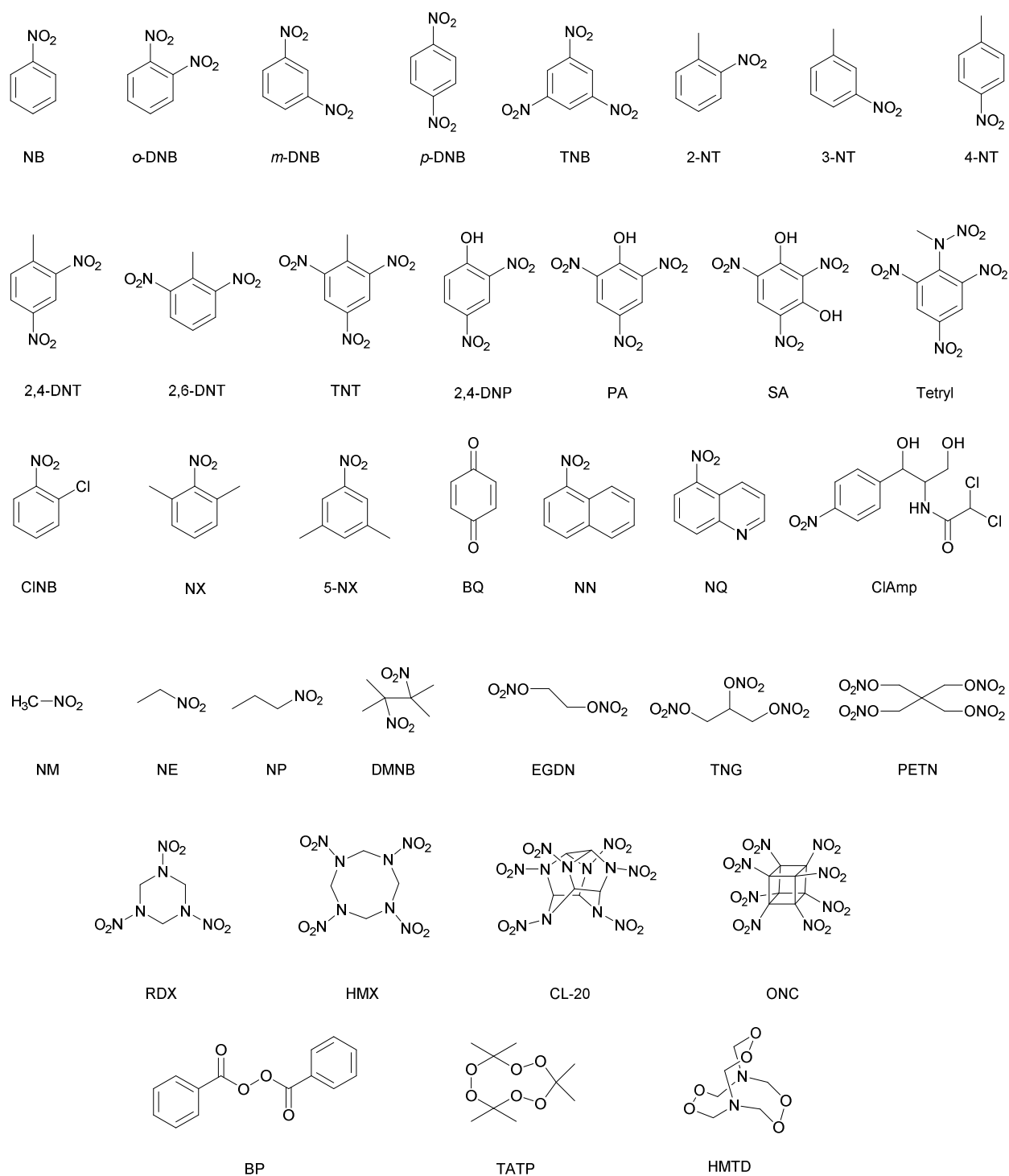


Figure 11. Selected molecular structures of explosives and explosive-like substances: NB (nitrobenzene), α -DNB (1,2-dinitrobenzene), m -DNB (1,3-dinitrobenzene), p -DNB (1,4-dinitrobenzene), TNB (1,3,5-trinitrobenzene), 2-NT (2-nitrotoluene), 3-NT (3-nitrotoluene), 4-NT (4-nitrotoluene), 2,4-DNT (2,4-dinitrotoluene), 2,6-DNT (2,6-dinitrotoluene), TNT (2,4,6-trinitrotoluene), 2,4-DNP (2,4-dinitrophenol), PA (picric acid), SA (Styphnic acid), Tetryl (2,4,6-Trinitrophenylmethylnitramine), CINB (2-chloronitrobenzene), NX (2-nitro- m -xylene), 5-NX (5-nitro- m -xylene), BQ (1,4-benzoquinone), NN (1-nitronaphthalene), NQ (5-nitroquinoline), ClAmp (chloramphenicol), NM (nitromethane), NE (nitroethane), NP (1-nitropropane), DMNB (2,3-dimethyl-2,3-dinitrobutane), EGDN (ethylene glycol dinitrate), TNG (trinitroglycerin), PETN (pentaerythritol tetranitrate), RDX (1,3,5-trinitro-1,3,5-triazacyclohexane), HMX (octahydro-1,3,5,7-tetranitro-1,3,5,7-tetrazocine), CL-20 (hexanitrohexaazaisowurtzitan), ONC (octanitrocubane), BP (benzoyl peroxide), TATP (triacetone triperoxide), HMTD (hexamethylene triperoxide diamine).

Table 2. Calculated HOMO and LUMO energy levels at B3LYP/6-31+G*.^{199 200}

| Group | Chemical Nature | Name | HOMO (eV) | LUMO (eV) |
|------------|-------------------------------|--|-----------|-----------|
| A | Electron Deficient Conjugated | cyanobenzene | -7.552 | -1.790 |
| | | 2-nitrotoluene (NT) | -7.555 | -2.747 |
| | | 1,4-dicyanobenzene | -8.029 | -2.871 |
| | | nitrobenzene (NB) | -7.888 | -2.915 |
| | | 2,4-dinitrotoluene (DNT) | -8.414 | -3.409 |
| | | 1,3-dinitrobenzene (<i>m</i> -DNB) | -8.731 | -3.597 |
| | | 2,4,6-trinitrotoluene (TNT) | -8.810 | -3.930 |
| | | 1,4-benzoquinone | -7.798 | -3.948 |
| | | 1,4-dinitrobenzene (<i>p</i> -DNB) | -8.661 | -3.955 |
| | | picric acid (PA) | -8.595 | -4.321 |
| B | Electron Rich Aromatic | durene | -6.097 | -0.065 |
| | | mesitylene | -6.429 | -0.190 |
| | | <i>o</i> -xylene | -6.504 | -0.205 |
| | | <i>m</i> -xylene | -6.491 | -0.262 |
| | | aniline | -5.718 | -0.282 |
| | | 4-ethyltoluene | -6.399 | -0.287 |
| | | <i>p</i> -xylene | -6.391 | -0.310 |
| | | toluene (TO) | -6.675 | -0.348 |
| | | ethylbenzene (Et-BZ) | -6.635 | -0.360 |
| | | anisole | -6.163 | -0.374 |
| | | benzene (BZ) | -6.995 | -0.393 |
| | | phenol | -6.314 | -0.482 |
| | | chlorobenzene (Cl-BZ) | -6.946 | -0.776 |
| | | bromobenzene (Br-BZ) | -6.841 | -0.787 |
| C | Electron Deficient Aliphatic | nitroethane (NE) | -8.396 | -2.331 |
| | | 1-nitropropane (NP) | -8.339 | -2.331 |
| | | nitromethane (NM) | -8.508 | -2.486 |
| | | 2,3-dimethyl-dinitrobutane (DMNB) | -8.620 | -2.853 |
| | | trinitroglycerin (TNG) | -9.494 | -2.934 |
| | | 1,3,5-trinitroperhydro-1,3,5-triazine (RDX) | -8.926 | -2.959 |
| | | octahydro-1,3,5,7-tetranitro-1,3,5,7-tetrazocine (HMX) | -8.740 | -3.053 |
| D | Others | water | -8.736 | 0.684 |
| | | methanol | -7.669 | 0.008 |
| | | ethanol | -7.569 | 0.005 |
| | | <i>N,N</i> -dimethylacetamide (DMA) | -6.700 | -0.084 |
| | | <i>N,N</i> -dimethylformamide (DMF) | -6.926 | -0.084 |
| | | butyronitrile | -8.967 | -0.138 |
| | | acetonitrile | -9.185 | -0.261 |
| | | 3-pentanone | -6.921 | -0.630 |
| | | 2-octanone | -6.932 | -0.663 |
| | | 2,4-dimethyl-3-pentanone | -6.731 | -0.717 |
| | | acetone | -7.027 | -0.746 |
| | | cycloheptanone | -6.734 | -0.768 |
| | | cyclopentanone | -6.790 | -0.834 |
| | | cyclohexanone | -6.742 | -0.839 |
| chloroform | -8.742 | -1.623 | | |

3.2 Detection in the Vapor Phase

In 2009 we reported the first study of using porous LMOF compounds for explosive detection.^{96, 201} Upon exposure of LMOF-111 (or RPM3-Zn, $Zn_2(\text{bpdc})_2(\text{bpee})\cdot 2\text{DMF}$, bpdc = 4,4'-biphenyldicarboxylate; bpee = 1,2-bis(4-pyridyl)ethylene) to the vapors of DNT (0.18 ppm, an evitable by-product in the manufacture of TNT) and DMNB (2.7 ppm, an explosive taggant) at room temperature, the fluorescence of an activated sample was drastically quenched more than 80% within 10s, as well as being red shifted (see Figure 12). The quenching percentage is defined as $(I_0 - I)/I_0 \times 100\%$, where I_0 is the original emission intensity and I is the intensity after exposure to analyte. LMOF-111 exhibits superb sensitivity for the

detection of DNT, and it has both a greater quenching effect and faster response time than the sensors based on conjugate polymers. The remarkable response from DMNB is also worth mentioning since DMNB is extremely difficult to detect with conjugate polymers due to the lack of π - π interactions. As a sensory material, LMOF-111 is also fully recyclable: the fluorescence of this material can be conveniently recovered by heating at 150 °C for one minute.

A systematic study on LMOF-121 ($Zn_2(\text{oba})_2(\text{bpy})\cdot \text{DMA}$, oba = 4,4'-oxybis(benzolate); bpy = 4,4'-bipyridine) covering a variety of analytes with different electronic properties revealed the possible fluorescence response mechanism that may be general for LMOFs.⁶² Electron deficient analytes quench the fluorescence of LMOF-121, while on the other hand electron

rich analytes enhance the fluorescence (Figure 13). The distinct behaviors from the two groups of analytes may be explained by the excited state electron transfer process. Reduction potential measurements and computational studies suggested that in the presence of an electron deficient analyte, electrons can transfer from LUMO/CB of LMOF-121 to the LUMO of the analyte upon excitation and then follow a non-radiative relaxation. This electron transfer pathway is responsible for the fluorescence quenching. In the encounter with an electron rich analyte, excited electrons can migrate from the high-lying LUMO of the analyte to the CB of LMOF-121, leading to an enhanced radiative band gap emission. Arguably, the adsorbed analyte can also inhibit the linker ligand's motions, such as rotation and vibration, which limits the non-radiative decay by a certain extent as seen in the cases of AIE, where restriction of intramolecular rotation and torsion leads to enhanced emission.^{24, 51, 63, 202, 203} In general, the nature of these photo-physicochemical processes is complicated, and there can potentially be more than one mechanism contributing to the same experimental phenomenon. Besides being able to differentiate analyte molecules based on their respective LUMO energies, LMOF-121 also has a strong preference for responding to aromatic compounds versus aliphatic analogues, since the orbital overlap from aromatic analytes is greater than that from aliphatic ones. This interesting feature makes LMOF-121 more selective towards aromatic analytes.

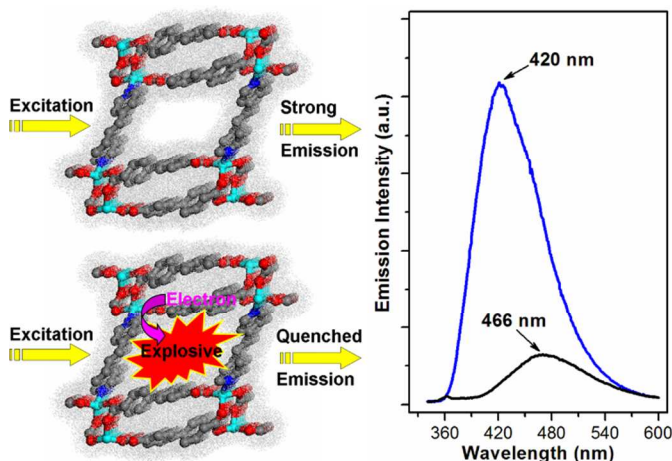


Figure 12. Left: An illustration of the fluorescence quenching due to analyte absorption and the subsequent electron transfer. Right: Fluorescence spectra before (blue) and after (black) exposure to the vapor of DMNB at room temperature for 10s. Reprinted with permission from ref 96. Copyright 2009 Wiley-VCH.

Additional studies on a series of LMOFs having strong emissions, LMOF-131 (or RPM1-Zn, $Zn_3(bpdc)_3(bpy) \cdot 4DMF \cdot H_2O$), LMOF-132 (or RPM7-Zn, $Zn_3(bpdc)_3(2,2'-dmbpy) \cdot 4DMF \cdot H_2O$, $2,2'$ -*dmbpy* = $2,2'$ -dimethyl-4,4'-bipyridine), LMOF-141 (or RPM4-Zn, $Zn_2(bpdc)_2(bpe) \cdot 2DMF$, *bpe* = 1,2-bis(4-pyridyl)ethane), and LMOF-151 (or RPM5-Zn, $Zn(bpdc)(bpe) \cdot DMF$) further confirmed their PL response to electron deficient and electron rich analytes.⁷² This series of LMOFs was built using similar

linker ligands but having different structures. The results show that they unanimously respond to electron deficient analytes through fluorescence quenching and to electron rich analytes through fluorescence enhancement. Electrochemical studies uncovered that electron deficient analytes usually have greater reduction potentials than LMOFs, which makes them excellent electron acceptors. On the contrary, reduction potentials of electron rich analytes are generally more negative, enabling them to donate electrons to LMOFs. This is in good agreement with the results of theoretical calculations, which show that the LUMO energy levels of electron-deficient analytes are lower than the CB of LMOFs, while those of electron-rich analytes lie above the CB of LMOFs. Very recently, a systematic study was also carried out on a paddle-wheel based LMOF series, including LMOF-161 ($Zn_2(ndc)_2(bpe) \cdot 2.25DMF \cdot 0.25H_2O$, *ndc* = 2,6-naphthalenedicarboxylate), LMOF-162 ($Zn_2(ndc)_2(bpee) \cdot 2.25 DMF \cdot 0.5H_2O$), LMOF-171 ($Zn_2(ndc)_2(ted) \cdot xDMF \cdot yH_2O$), and LMOF-181 ($Zn_2(ndc)_2(bpy) \cdot xDMF$).⁷¹ The same observations and trends were found, offering support to the aforementioned electron transfer mechanism.

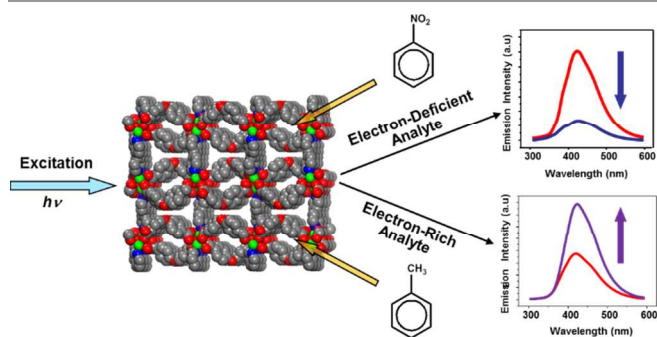


Figure 13. An illustration of fluorescence response: quenching induced by the electron deficient nitrobenzene, and enhancement induced by the electron rich toluene.

Although it is well established by now that electron-deficient analytes quench and electron-rich analytes enhance the photoluminescence of sensory materials respectively as observed independently by several research groups,^{62, 71-73, 95} solely monitoring the change in their emission intensity is usually insufficient for accurate and selective detection of a targeted species, especially when more than one analyte molecules quench or enhance the fluorescence to a similar extent. A change in emission frequency (wavelength) can sometimes be utilized as an additional sensing/detection parameter. Although not as common as changes in fluorescence intensity, strong analyte-sensor interactions often lead to emission frequency shifts. Monitoring the changes in both fluorescence intensity and frequency adds a new variable of signal transduction: from one-dimension (1D) to two-dimensions (2D), where both sensitivity and selectivity can be greatly enhanced. In an effort to minimize false-positive responses and increase selectivity, this 2D strategy was exemplified using two highly fluorescent and structurally related LMOFs.⁷⁰ Diverse groups of analytes were tested on

LMOF-161 and LMOF-162.²⁰⁴ Both LMOFs demonstrate a 2D response: fluorescence intensity change paired with emission frequency shift. Utilizing both variables, an analyte can be pinpointed on a two-dimensional map as shown in Figure 14. The change in fluorescence intensity is expected to be governed by the previously discussed electron transfer mechanism. In-situ IR studies, featuring the shifts in the signature vibrational modes of free analytes and adsorbed analytes, unraveled the intrinsic electron flow from LMOF to electron deficient compound, and from electron rich compound to LMOF. This observation further supports the donor-acceptor electron transfer mechanism discussed earlier. Computational studies indicate that upon analyte perturbation, the band structure of the analyte-LMOF exciplex system differs from that of the LMOF, and therefore a change in emission frequency is observed. As a proof of concept, the 2D map strategy can be of great assistance in the accurate recognition of analytes and may lead to differentiation between analytes with extremely similar physicochemical properties.

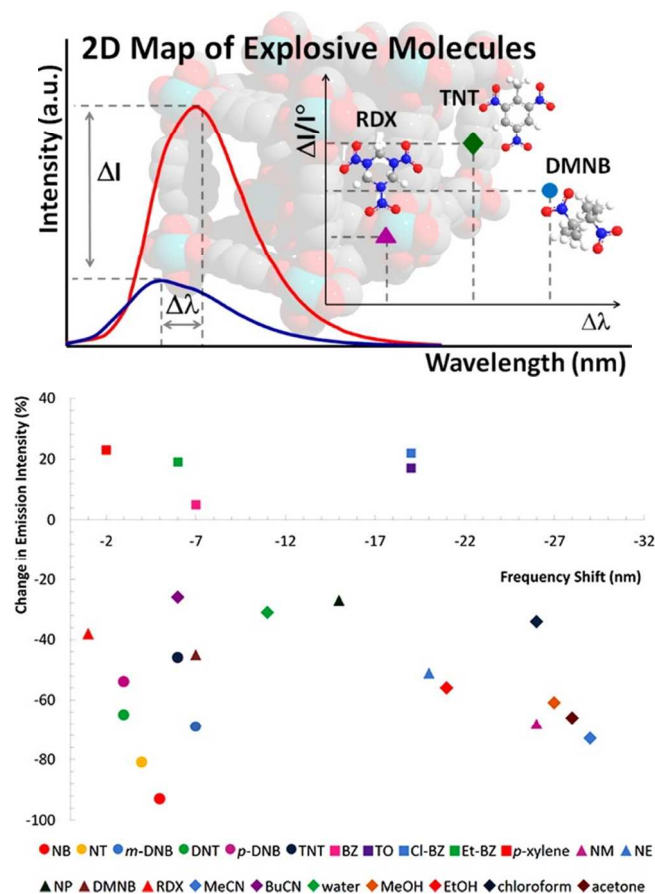


Figure 14. Top: An illustration of the analyte-induced two dimensional response: $\Delta\lambda$ and ΔI . And the generation of a 2D map. Bottom: A 2D color-coded map of analyte recognition by LMOF-162. Reprinted with permission from ref 70. Copyright 2013 American Chemical Society.

The rational design of effective sensory materials requires the understanding of analyte-sensor interactions. Direct experimental evidence of the interaction between nitrobenzene and a Li-based LMOF, $\{Li_3[Li(DMF)_2](cpma)_2\} \cdot 4DMF \cdot H_2O$,

was observed in a single crystal sample containing the nitrobenzene analyte: strong π - π stacking with neighboring ligands enabled by the confinement of nitrobenzene in the pore channel, and interaction between the nitro group and benzene ring of the ligand (suggested by the close $N_{nitro} \cdots C_{ligand}$ distance) results in the strong quenching of fluorescence coupled with a color change of the single crystal.⁸¹ In another example, single crystal structural data showed trapped guest molecules in a 2D π -stacked LMOF, $[Zn_{1.5}(L^{10})(H_2O)] \cdot 1.5BZ$ (BZ = benzene).⁹⁴ As shown in Figure 15c, adsorbed benzene is trapped between the adjacent 2D layers forming a π -complex with the LMOF. It was extrapolated that the quencher molecule, like nitrobenzene, mainly gets absorbed on the π -electron rich surface of the LMOF, where the fluorescence quenching is facilitated by the supramolecular wire effect of the π -stacks.

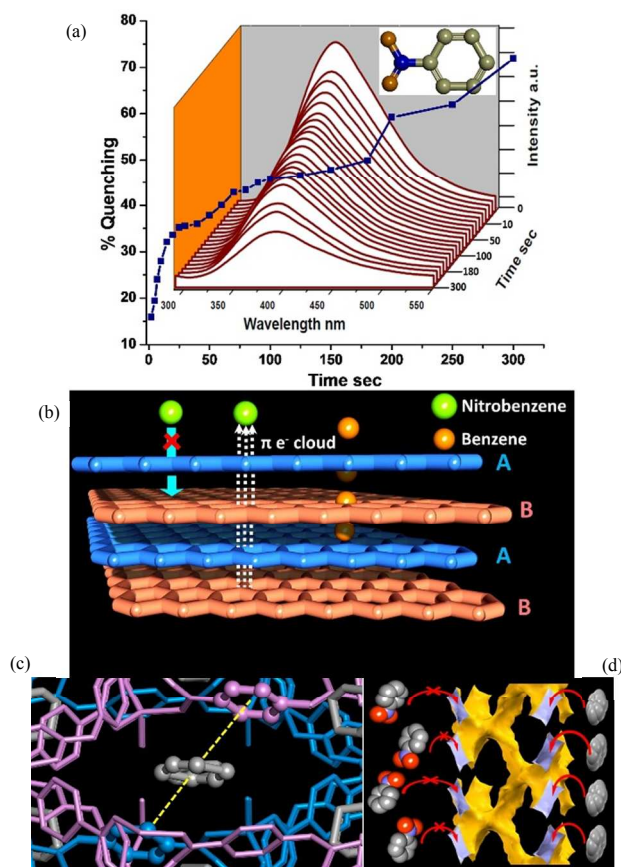


Figure 15. (a) The time-dependent fluorescence quenching profile of a 2D MOF, $[Zn_{1.5}(L^{10})(H_2O)] \cdot 1.5BZ$, by nitrobenzene. (b) Supramolecular wire effect of $[Zn_{1.5}(L^{10})(H_2O)] \cdot 1.5BZ$, displaying the flow of π -electrons between sheets, the possible diffusion of benzene, and the surface interaction of nitrobenzene. (c) Structure of the 2D LMOF showing the formation of a π -complex with benzene between the π -electron clouds of two sheets. (d) An illustration of four benzenes in the framework with different orientations and nitrobenzene being excluded by the framework. Reprinted with permission from Ref 94. Copyright 2013 American Chemical Society.

Theoretical and computational studies can offer insights pertaining to the origin of a sensor's luminescence, the PL response, as well as the possible interaction sites.²⁰⁵⁻²¹¹ For example, band structure calculations are extremely useful in understanding the electron transfer mechanism, where the

relative position of an LMOF's CB and an analyte's LUMO determines the direction of electron transfer.^{62, 71, 72, 94} Ghosh et al. found that the analyte with lowest LUMO coincided with the strongest quenching effect, based on their experiment.⁶⁶ Odbadrakh et al. investigated the physisorption of RDX on the surface and in the pores of IRMOF-1 by employing density functional theory (DFT): the binding site in the pore lies on the ligand, while on the surface RDX mostly interacts with the metal sites.²⁰⁶ Keffer and coworkers performed quantum mechanical calculations, classical grand canonical Monte Carlo simulations (GCMC), and classical molecular dynamics simulations to study the effect of charge distribution on the adsorption of RDX in IRMOF-10.²⁰⁷ Overall, studies on the electron transfer mechanism and analyte-LMOF interactions have provided great insight for improving the rational design of effective sensors.

LMOFs as explosive sensors are truly versatile: not only can they probe analytes in the vapor phase, but they have also proven to be feasible and effective in liquid phase detection. Chen and Qian et al. utilized $\text{Eu}_2(\text{bdc})_3(\text{H}_2\text{O})_2(\text{H}_2\text{O})_2$ for the detection of DNT and TNT in ethanol.¹³⁸ Mukherjee et al. demonstrated the effective fluorescence quenching of $[\text{Zn}_4\text{O}(\text{L}^{13})_2(\text{H}_2\text{O})_3]\cdot 3\text{DMA}\cdot 3\text{EtOH}\cdot 6\text{H}_2\text{O}$ by TNT in ethanol.¹³⁸ Shi et al. studied the PL quenching of $[\text{Zn}_3(\text{tdpat})(\text{H}_2\text{O})_3]$ with the addition of nitrobenzene in methanol.¹⁰⁷ Du, Chen and coworkers investigated the PL response of $[\text{In}_2\text{L}^{29}][\text{NH}_2(\text{CH}_3)_2]_2(\text{DMF})_4(\text{H}_2\text{O})_{16}$ upon the addition of different analytes (electron deficient or rich) in DMF.¹³⁰

As established previously, the short-ranged electron transfer between a sensory material and analyte largely determines the fluorescence response. Tuning the band structure of an LMOF to facilitate this process is an important and logical consideration for the design of an effective sensor. However, due to the insulating nature of most LMOFs and generally weak host-guest interactions, the electron transfer process is limited by orbital or spatial overlaps of the framework and analyte, and thus, may impede the performance of LMOF-based sensors. Energy transfer on the other hand, is a long-range process and does not require a conductive medium. Optimizing both factors is the key to achieving superb performance. This was demonstrated by Nagarkar and coworkers with $[\text{Cd}(\text{ndc})_{0.5}(\text{pca})]\cdot x\text{G}$ (G = guest molecules, pca = 4-pyridinecarboxylic acid). The combination of both effective electron and energy transfer led to a sensory profile with excellent sensitivity and selectivity.⁶⁶ The LMOF was preferentially quenched by TNP (or 2,4,6-trinitrophenol or picric acid) in MeCN, while exposure to other nitro compounds had little effect on its fluorescence intensity (Figure 16). The k_{sv} for TNP is as high as $3.5 \times 10^4 \text{ M}^{-1}$, a value comparable to the best conjugate polymer sensors. Such high sensitivity and selectivity was attributed to several factors. First, TNP has the lowest LUMO energy of all the analytes studied, which makes it the strongest electron acceptor in the excited state. Second, the Lewis basic sites from pca can interact effectively with the acidic phenolic protons from TNP. These acid-base interactions attract the TNP molecules to be in closer proximity to the sensor. Finally, the spectral overlap between the optical emission spectrum of the LMOF and the optical absorption spectrum of TNP is significantly greater than the overlap from the other nitro compounds. Thus, the strongly amplified quenching effect is a result of combined short-ranged electron transfer and long-range energy transfer process.

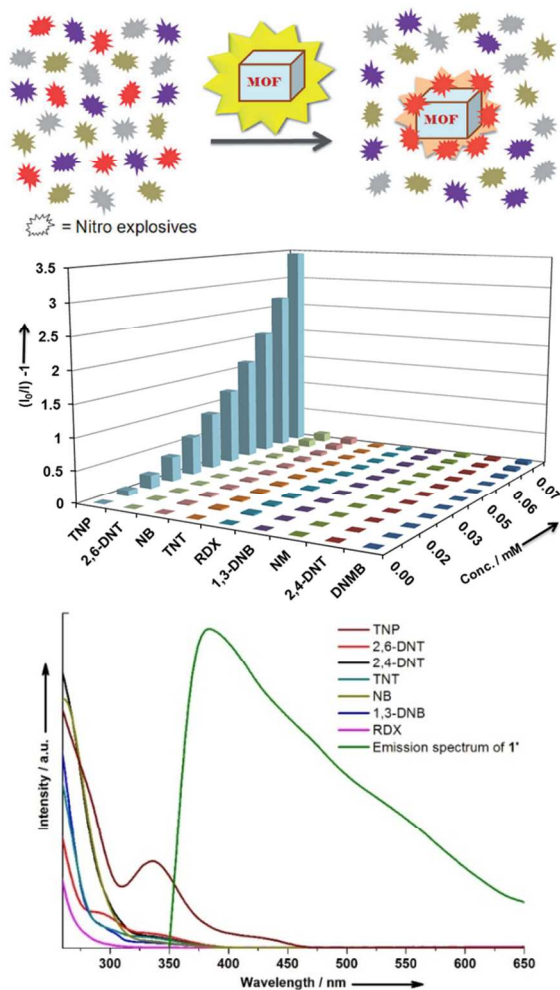


Figure 16. Top: An illustration of an LMOF-based sensor, $[\text{Cd}(\text{ndc})_{0.5}(\text{pca})]$, for the selective detection of aimed nitro explosive. Middle: Stern-Volmer plots for various analytes. Bottom: Spectral overlap between the emission spectrum of the LMOF (green solid line) and the absorption spectra of analytes Adapted with permission from Ref 66. Copyright 2013 Wiley-VCH.

3.3 Detection in the Liquid Phase

3.4 Detection with Nanosized LMOFs

Decreasing the size of LMOF particles to the nanometer scale (NLMOFs) is a powerful approach to promote faster response time. Zhang and coworkers demonstrated that with the nanosized Zn-bcpa (bcpa = 9, 10-bis(p-carboxyphenyl)anthracene) fast detection of DNT and TNT in the vapor phase can be achieved through fluorescence quenching.²¹² Qiu et al. used a self-sacrificing template route to synthesize MOF

nanotubes (MOFNTs) as shown in Figure 17.¹²³ The resulting MOFNTs showed a fast, selective, and reversible response to the vapor of DNT. In the case of LMOF-161, surfactant assisted method was used to decrease the particle size. Shorter response time was achieved to obtain emission shifts.⁷⁰ Chen, Qian and coworkers utilized the water-in-oil microemulsion strategy to synthesize nanorods of $\text{Eu}_2(\text{bdc})_3(\text{H}_2\text{O})_2(\text{H}_2\text{O})_2$ (bdc = benzene-1,4-dicarboxylate), which showed high sensitivity for nitroaromatic explosives in ethanol solution.¹³⁸ Other methods, such as microwave and surfactant assisted synthesis, can also lead to the formation of nanoscale materials. Generally speaking, downsizing LMOF particles contributes greatly to enhancing sensory performance in both response time (faster kinetics) and response magnitude.

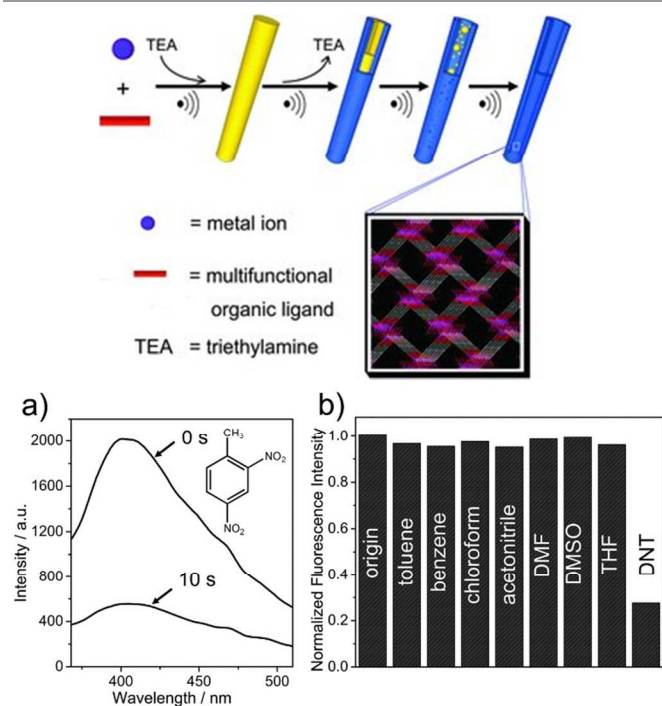


Figure 17. Top: An illustration of the self-sacrificing template strategy for the synthesis of MOFNTs. Bottom: (a) Fluorescence quenching of the MOFNTs by the vapor of DNT after 10 s. exposure (b) Fluorescence intensities of MOFNTs after exposures to different analytes (comparing to the original). Reprinted with permission from Ref 123. Copyright 2012 Wiley-VCH.

3.5 Indirect Detection of Non-Volatile High Explosives

High explosives such as RDX and HMX have extremely low vapor pressures that make their effective detection one of the most challenging tasks. However, volatile components in these plastic explosives, such as solvents, stabilizers, and plasticizers, make easier targets. Therefore, detection of these volatile components serves as an alternative route for the identification of high explosives.^{213, 214}

Adapting the 2D mapping strategy, LMOF-202 ($\text{Zn}_2(\text{hfdc})_2(\text{bpy}) \cdot x\text{DMA}$, hfdc = 9H-fluorene-2,7-dicarboxylic acid) was demonstrated to be capable of rapid and selective detection of cyclohexanone, a solvent used in the recrystallization of RDX and coexisting in the product

mixture.²⁰⁰ The fluorescence intensity of LMOF-202' (guest free LMOF-202) was greatly enhanced after only 10 seconds of exposure to the vapors of various ketones. Additionally, the emission frequency was also altered after analyte exposure. By utilizing both signals, each ketone can be pin-pointed on a 2D map. Molecular orbital calculations revealed that the high-lying LUMO orbitals of the ketones facilitate the electron transfer to the CB of LMOF-202'. Further investigation of the electronic properties of the LMOF and analytes unraveled another important factor that also contributes to the fluorescence enhancement: large spectral overlap found between the absorbance of LMOF-202' and the emission of the ketones allows for effective energy transfer (Figure 18a) and, therefore, contributes largely to the fluorescence enhancement. On the other hand, LMOF-121', a MOF structure with similar porosity as LMOF-202', exhibits a significantly lower percentage of PL enhancement upon analyte exposure of the same duration. This can be explained by the decreased spectral overlap shown in Figure 18a. Such observations further confirm that energy transfer plays an equally important role in fluorescence response.

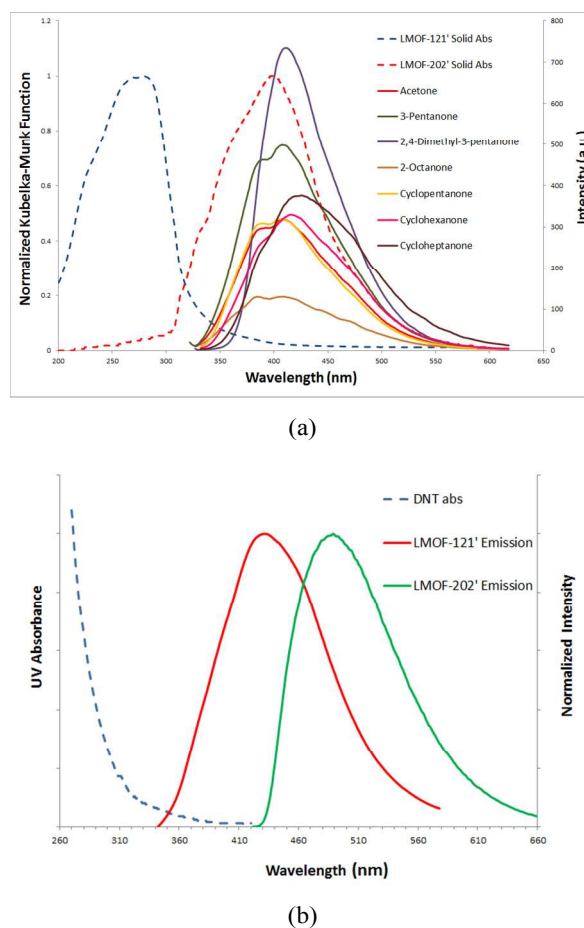


Figure 18. (a) Dashed line: Optical absorbance of LMOF-121' and LMOF-202'. Solid line: Emission spectra of ketones. (b) Optical absorbance of DNT (dashed line) and emission spectra of LMOF-121' and LMOF-202' (solid line).

On the other hand, both LMOF-121 and -202 respond to DNT through fluorescence quenching. Notably, the K_{sv} of LMOF-121 is 2.3 times of that of LMOF-202. This is most likely due to the noticeable spectral overlap found between the absorbance of DNT and the emission of LMOF-121, while such overlap is nearly negligible for LMOF-202 (see Figure 18b). This observation again confirms energy transfer is a significant factor in governing fluorescence response. A closely related structure, LMOF-201 ($Zn_2(\text{ofdc})_2(\text{bpy}) \cdot 2.5\text{DMF} \cdot 1.25\text{H}_2\text{O}$, ofdc = 9-oxo-9H-fluorene-2,7-dicarboxylic acid), has a very similar band gap to LMOF-202, but is nearly nonporous and therefore inert to the vapors of ketones. Overall, the porosity and electronic properties of an LMOF are both important factors influencing its performance. High porosity facilitates the analyte diffusion and tuning the electronic property can enable effective energy transfer.

LMOFs are excellent candidates for explosive detection. The combination of effective electron and energy transfers is a powerful way to achieve highly sensitive and selective detection. In addition, making use of the porosity of LMOF structures and incorporating functional groups into their frameworks can promote analyte-sensor interactions, while decreasing the particle size will reduce response time substantially. All of these factors play important roles and should be considered in the future synthesis of LMOFs for further enhanced performance.

4. Conclusions

Metal-organic frameworks are a truly versatile and remarkable class of crystalline functional materials with many interesting properties and great potential for numerous applications. The photoluminescence of these materials arises from several charge transfer processes: LMCT, MLCT, LLCT, and metal centered with antenna ligands. Utilizing their emission properties, various types of sensors are being developed. From the detection of small molecules, VOCs, and ionic species, to biosensing and imaging, and fluorescent thermometers, luminescence based sensing has been applied to various fields. The optical signal can be either monitored by a fluorometer in terms of changes in intensity or emission frequency, or can be seen by the naked eye in the case of colorimetric response. A highly promising area of luminescence based sensing is the detection of explosives and explosive-like molecules. Effective fluorescence response in the vapor and/or liquid phases can be achieved through the rational design of sensory materials with strong electron and energy transfers, suitable porosity and particle size, specific functional groups, and tunable electronic structures for highly selective analyte-LMOF interactions. For instance, raising the LUMO (or CB) of LMOF favors the electron transfer to the low-lying LUMO of electron deficient analyte during an excitation process and therefore promotes fluorescence quenching. Tuning the band gap of LMOF to increase the spectral (emission and absorption or vice versa) overlap between LMOF and analyte can enhance energy transfer. The incorporation of LBS, OMS or other functional groups facilitates specific LMOF-analyte interaction. It is anticipated that with continued efforts in the design, synthesis and optimization of new materials, LMOF-based sensors are on their way to commercialized applications.

Acknowledgements

The authors are grateful for the financial support from the Department of Energy, Basic Energy Sciences, division of Materials Sciences and Engineering via Grant No. DE-FG02-08ER46491.

List of Abbreviations

(acidic hydrogens are ignored with respect to alphabetizing)

| | |
|-------------------------------------|---|
| 1 ⁴⁺ | tetracationic macrocycle |
| 1D | one-dimensional |
| 2,2'-dmbpy | 2,2'-dimethyl-4,4'-bipyridine |
| 2,4-DNT | 2,4-dinitrotoluene |
| 2,4-DNP | 2,4-dinitrophenol |
| 2,6-DNT | 2,6-dinitrotoluene |
| 2,6-pdc | pyridine-2,6-dicarboxylate |
| 2D | two-dimensional |
| 2-NT | 2-nitrotoluene |
| 3,5-Na ₂ Hdsb | 3,5-disulfobenzoic acid disodium salt |
| 3D | three-dimensional |
| 3-Hptt | 5-(pyridin-3-yl)-1H-1,2,4-triazole-3-thiol |
| 3-NT | 3-nitrotoluene |
| 3-tymntb | tris((pyridin-3-ylmethyl)benzimidazol-2-ylmethyl)amine |
| 4,4'-bipy | 4,4'-bipyridine |
| 4-NT | 4-nitrotoluene |
| 5-NX | 5-nitro- <i>m</i> -xylene |
| AA-PEG | anisamide polyethylene glycol |
| ad | adeninate |
| AFPs | amplifying fluorescent polymers |
| A-GO | acid-functionalized graphene oxide |
| AIE | aggregation induced emission |
| Alq3 | tris-(8-hydroxyquinoline)aluminum |
| amp | adenosine monophosphate |
| azpy | 4,4'-azobipyridine |
| Hba | benzoic acid |
| H ₂ bcpa | 9,10-bis(<i>p</i> -carboxyphenyl)anthracene |
| H ₂ bdc | 1,4-benzenedicarboxylic acid (also terephthalic acid) |
| H ₂ bibdc | 4,4'-biphenyldicarboxylic acid |
| BINOL | 1,1'-bi-2-naphthol |
| bipy | 4,4'-bipyridine |
| BP | benzoyl peroxide |
| bpa | 4,4'-bis(4-pyridyl)ethane |
| bpdc | 4,4'-biphenyldicarboxylate |
| H ₂ bpdc* | 2,2'-bipyridine-3,3'-dicarboxylic acid |
| bpe | 1,2-bis(4-pyridyl)ethane |
| bpee | 1,2-bipyridylethane |
| H ₃ bpt | biphenyl-3,4',5-tricarboxylic acid |
| bpy | 4,4'-bipyridine |
| H ₂ bpybcCl ₂ | 1,1'-bis(4-carboxybenzyl)-4,4'-bipyridinium dichloride |
| BQ | 1,4-benzoquinone |
| H ₂ bqdc | 2,2'-biquinoline-4,4'-dicarboxylic acid |
| Br-BZ | bromobenzene |
| H ₃ btb | 1,3,5-tris(4-carboxyphenyl)benzene |
| H ₃ btc | 1,3,5-benzenetricarboxylic acid |
| H ₂ btca | benzotriazole-5-carboxylic acid |
| H ₃ btcpa | 1,1',1''-(benzene-1,3,5-triyl)tripiperidine-4-carboxylic acid |
| BZ | benzene |
| CB | conduction band |
| CL-20 | hexanitrohexaazaisowurtzitane |

| | | | |
|--------------------------------|--|--------------------------------|--|
| ClAmp | chloroamphenicol | L ¹² | N,N'-bis-(4-pyridyl)phthalamide |
| Cl-BZ | chlorobenzene | H ₃ L ¹³ | 5-(4-carboxyphenylethynyl)isophthalic acid |
| CINB | 2-chloronitrobenzene | L ¹⁴ | 4',4'',4'''-(2,4,6-trimethylbenzene-1,3,5-triyl)tris(methylene)tribiphenyl-4-carboxylate |
| H ₂ cpeip | 5-((4-carboxyphenyl)ethynyl)isophthalic acid | | |
| H ₂ cpma | bis(4-carboxyphenyl)-N-methylamine | H ₈ L ¹⁵ | 5,5'-(2,2-bis((3,5-dicarboxyphenoxy)methyl)propane-1,3-diyl)bis(oxy)diisophthalic acid |
| H ₃ cpoip | 4-(2-carboxyphenoxy)isophthalic acid | | |
| dabco | 1,4-diazabicyclo[2.2.2]octane (also ted: triethylenediamine) | H ₂ L ¹⁶ | 2,5-dithioalloxyterephthalic acid |
| DEF | N,N-diethylformamide | L ¹⁷ | N ⁴ ,N ⁴ -di(pyridin-4-yl)biphenyl-4,4'-dicarboxamide |
| DFT | density functional theory | | |
| H ₂ dhbdc | 2,5-dihydroxybenzene-1,4-dicarboxylic acid (also H ₂ dht: 2,5-dihydroxyterephthalic acid) | L ¹⁸ | (1E,1'E)-N,N'-(ethane-1,2-diylbis(4,1-phenylene))bis(1-(pyridin-2-yl)methanimine) |
| H ₂ dht | 2,5-dihydroxyterephthalic acid (also H ₂ dhbdc: 2,5-dihydroxybenzene-1,4-dicarboxylic acid) | H ₂ L ¹⁹ | trans-4,4'-stilbenedicarboxylic acid |
| H ₂ dht*/dht* | 2,5-dihydroxyterephthalate/2,5-dioxidoterephthalate | H ₂ L ²⁰ | 5-(benzyloxy)isophthalic acid |
| DMA | N,N-dimethylacetamide | H ₂ L ²¹ | 5-(naphthalen-1-ylmethoxy)isophthalic acid |
| H ₂ dmbdc | 2,5-dimethoxy-1,4-benzenedicarboxylic acid | H ₂ L ²² | 5-(pyren-1-ylmethoxy)isophthalic acid |
| H ₂ dmbd | 2,5-dimercapto-1,4-benzenedicarboxylic acid | H ₂ L ²³ | [Ru{5,5'-(CO ₂) ₂ -bpy}(bpy) ₂] |
| DMF | N,N-dimethylformamide | H ₄ L ²⁴ | Ru(5,5'-CO ₂ H-bpy) ₂ CN ₂ |
| DMNB | 2,3-dimethyl-dinitrobutane | L ²⁵ | 4-cyanobenzoate |
| Hdmp | 3,5-dimethyl-4-(4'-pyridyl)pyrazole | L ²⁶ | 3,5-bis(3-carboxyphenyl)-1,2,4-triazole |
| <i>m</i> -DNB | 1,3-dinitrobenzene | L ²⁷ | 4-amino-3,5-bis(4-pyridyl-3-phenyl)-1,2,4-triazole |
| <i>o</i> -DNB | 1,2-dinitrobenzene | H ₄ L ²⁸ | (R)-2,2-dihydroxy-1,1'-binaphthyl-4,4',6,6'-tetrakis(4-benzoic acid) |
| <i>p</i> -DNB | 1,4-dinitrobenzene | H ₈ L ²⁹ | tetrakis[(3,5-dicarboxyphenoxy)methyl]methane |
| DNT | 2,4-dinitrotoluene | H ₃ L ³⁰ | 4,4'-((2-((4-carboxyphenoxy)methyl)-2-methylpropane-1,3-diyl)bis(oxy))dibenzoic acid |
| DPA* | dipicolinic acid | | |
| H ₂ dpa | 2,6-pyridinedicarboxylic acid | H ₄ L ³¹ | 5-(3,5-dicarboxybenzyloxy)isophthalic acid |
| dpb | 1,4-di(4-pyridyl)benzene | H ₄ L ³² | tetrakis[4-(carboxyphenyl)oxamethyl]methane acid |
| EDXRD | energy dispersive X-ray diffraction | | |
| ee | enantiomeric excess | L ³³ | 2',5'-bis(methoxymethyl)-[1,1':4',1''-terphenyl]-4,4''-dicarboxylate |
| EGDN | ethylene glycol dinitrate | | |
| Et-BZ | ethylbenzene | HL ³⁴ | 4'-(4-carboxyphenyl)-2,2': 6',2''-terpyridine |
| EtOH | ethanol | H ₄ L ³⁵ | 4,4',4'',4'''-{2,2',2'',2'''-[ethane-1,2-diylbis(azanetriyl)]tetrakis(methylene)tetrakis(1 <i>H</i> -benzo-[<i>d</i>]imidazole-2,1-diyl)}tetrakis(methylene)-tetrabenzoic acid |
| eV | electron volts | | |
| H ₃ fbpt | 2'-fluorobiphenyl-3,4',5-tricarboxylic acid | | |
| H ₂ fda | furane-2,5-dicarboxylic acid | | |
| H ₂ fma | fumaric acid | H ₆ L ³⁶ | hexakis[4-(carboxyphenyl)oxamethyl]-3-oxapentane |
| G | guest molecules | | |
| GC | gas chromatography | H ₂ L ³⁷ | 2-(4-pyridinyl)-1 <i>H</i> -imidazole-4,5-dicarboxylic acid |
| GCMC | grand canonical Monte Carlo | | |
| HMTD | hexamethylene triperoxide diamine | LBS | Lewis basic site |
| HMX | octahydro-1,3,5,7-tetranitro-1,3,5,7-tetrazocine | LLCT | ligand-to-ligand charge transfer |
| Him | imidazole | LMCT | ligand-to-metal charge transfer |
| H ₃ imdc | 4,5-imidazoledicarboxylic acid | LMOFs | luminescent metal-organic frameworks |
| IMS | ion mobility spectrometry | MeCN | acetonitrile |
| L ¹ | 2,6-bis((3,5-dimethyl-1 <i>H</i> -pyrazol-4-yl)methyl)pyridine | Meim | 2-methylimidazolone |
| L ² | 3-(4-pyridyl)-5-(<i>p</i> -tolyl)pyrazolate | MeOH | methanol |
| L ³ | 3-(4-pyridyl)-5-(2,4-dimethylphenyl)pyrazolate | H ₂ mfd | 9,9-dimethylfluorene-2,7-dicarboxylic acid |
| H ₄ L ⁴ | 4,4'-(2,2-bis((4-carboxy-2-methoxyphenoxy)methyl)propane-1,3-diyl)bis(oxy)bis(3-methoxybenzoic acid) | mip ²⁻ | 5-methylisophthalate dianion |
| H ₆ L ⁵ | 1,2,3,4,5,6-hexakis(3-carboxyphenyloxymethylene)benzene | MLCT | metal-to-ligand charge transfer |
| H ₄ L ⁶ | biphenyl-3,3',4,4'-tetracarboxylic acid | MOFNTs | metal-organic framework nanotubes |
| H ₄ L ⁷ | 4,4'-oxydiphthalic acid | MOFs | metal-organic frameworks |
| L ⁸ | 4-[3-(4-carboxyphenoxy)-2-[(4-carboxyphenoxy)methyl]-2-methyl-propoxy]benzoate | mpba ⁴⁻ | N,N'-1,3-phenylenebis(oxamate) |
| L ⁹ | 1,4-bis(1-imidazolyl)benzene | MV ²⁺ | methylviologen dicationic dye |
| L ¹⁰ | 4,4',4''-(benzene-1,3,5-triyltris(oxy))tribenzoate | NB | nitrobenzene |
| H ₄ L ¹¹ | N-phenyl-N'-phenylbicyclo[2,2,2]oct-7-ene-2,3,5,6-tetracarboxdiimide tetracarboxylic acid | NCPs | nanoscale coordination polymers |
| | | H ₂ ndc | 2,6-naphthalenedicarboxylic acid |
| | | NE | nitroethane |
| | | NLMOFs | nanoscale luminescent metal-organic frameworks |
| | | NM | nitromethane |
| | | NN | 1-nitronaphthalene |
| | | NO | nitric oxide |
| | | NP | 1-nitropropane |

| | |
|----------------------|--|
| NQ | 5-nitroquinoline |
| NT | 2-nitrotoluene |
| NX | 2-nitro- <i>m</i> -xylene |
| H ₂ oa | oxalic acid |
| H ₂ oba | 4,4'-oxydibenzoic acid |
| Hoca-OH | (<i>E</i>)-3-(2-hydroxyl-phenyl)-acrylic acid |
| H ₂ oda | oxydiacetic acid |
| OMS | open metal site |
| ONC | octanitrocubane |
| Hox | oxalic acid |
| PA | picric acid (also TNP: 2,4,6-trinitrophenol) |
| Hpca | 4-pyridinecarboxylic acid |
| H ₂ pda | pyridine-2,6-dicarboxylic acid |
| H ₂ pdca | pyridine-3,5-dicarboxylic acid |
| PDMS | plasma desorption mass spectrometry |
| PETN | pentaerythritol tetranitrate |
| phen | phenanthroline |
| H ₂ pia | 5-(pyridin-4-yl)isophthalic acid |
| PL | photoluminescence |
| PXRD | powder X-ray diffraction |
| RDX | 1,3,5-trinitroperhydro-1,3,5-triazine |
| RPM | Rutgers recyclable porous material |
| SA | Styphnic acid |
| SBU | secondary building unit |
| SERS | surface enhanced Raman spectroscopy |
| H ₂ tart | L-tartaric acid |
| H ₃ tatb | 4,4',4''-s-triazine-2,4,6-triyltribenzoic acid |
| TATP | triacetone triperoxide |
| H ₆ tatpt | 2,4,6-tris(2,5-dicarboxylphenylamino)-1,3,5-triazine |
| H ₃ tca | tricarboxytriphenylamine |
| H ₃ tcpm | tris-(<i>p</i> -carboxyphenyl)-methane |
| H ₂ tcepe | tetrakis(4-carboxyphenyl)ethylene |
| H ₂ tcpp | tetrakis(4-carboxyphenyl)porphyrin |
| H ₆ tdpat | 2,4,6-tris(3,5-dicarboxyphenylamino)-1,3,5-triazine |
| ted | triethylenediamine (also dabco: 1,4-diazabicyclo[2.2.2]octane) |
| Tetryl | 2,4,6-trinitrophenylmethylnitramine |
| TGA | thermogravimetric analysis |
| tib | 1,3,5-tris(1-imidazolyl)benzene |
| TNB | 1,3,5-trinitrobenzene |
| TNG | trinitroglycerin (also NG: nitroglycerin) |
| TNP | 2,4,6-trinitrophenol (also PA: picric acid) |
| TNT | 2,4,6-trinitrotoluene |
| TO | toluene |
| tpe | tetraphenylethylene |
| H ₃ ttaa | N,N',N''-1,3,5-triazine-2,4,6-triyltris(4-aminomethylbenzoic acid) |
| VOCs | volatile organic compounds |
| XRD | X-ray diffraction |

Notes and references

Department of Chemistry and Chemical Biology, Rutgers University, 610 Taylor Road, Piscataway, NJ 08854, USA. Fax: (+01) 732-445-5312; Tel: (+01) 732-445-3758; E-mail: jingli@rutgers.edu

† Footnotes should appear here. These might include comments relevant to but not central to the matter under discussion, limited experimental and spectral data, and crystallographic data.

Electronic Supplementary Information (ESI) available: [details of any supplementary information available should be included here]. See DOI: 10.1039/b000000x/

- J. J. Perry Iv, J. A. Perman and M. J. Zaworotko, *Chem. Soc. Rev.*, 2009, **38**, 1400-1417.
- M. O'Keeffe and O. M. Yaghi, *Chem. Rev.*, 2012, **112**, 675-702.
- H. Furukawa, K. E. Cordova, M. O'Keeffe and O. M. Yaghi, *Science*, 2013, **341**.
- M. Li, D. Li, M. O'Keeffe and O. M. Yaghi, *Chem. Rev.*, 2013.
- T. R. Cook, Y.-R. Zheng and P. J. Stang, *Chem. Rev.*, 2013, **113**, 734-777.
- C. Janiak, *Dalton Transactions*, 2003, 2781-2804.
- S. T. Meek, J. A. Greathouse and M. D. Allendorf, *Adv. Mater.*, 2011, **23**, 249-267.
- L. J. Murray, M. Dinca and J. R. Long, *Chem. Soc. Rev.*, 2009, **38**, 1294-1314.
- T. A. Makal, J.-R. Li, W. Lu and H.-C. Zhou, *Chem. Soc. Rev.*, 2012, **41**, 7761-7779.
- M. P. Suh, H. J. Park, T. K. Prasad and D.-W. Lim, *Chem. Rev.*, 2012, **112**, 782-835.
- K. Sumida, D. L. Rogow, J. A. Mason, T. M. McDonald, E. D. Bloch, Z. R. Herm, T.-H. Bae and J. R. Long, *Chem. Rev.*, 2012, **112**, 724-781.
- J.-R. Li, J. Sculley and H.-C. Zhou, *Chem. Rev.*, 2012, **112**, 869-932.
- H. Wu, Q. Gong, D. H. Olson and J. Li, *Chem. Rev.*, 2012, **112**, 836-868.
- Z. Zhang, Y. Zhao, Q. Gong, Z. Li and J. Li, *Chem. Commun.*, 2013, **49**, 653-661.
- P. Nugent, Y. Belmabkhout, S. D. Burd, A. J. Cairns, R. Luebke, K. Forrest, T. Pham, S. Ma, B. Space, L. Wojtas, M. Eddaoudi and M. J. Zaworotko, *Nature*, 2013, **495**, 80-84.
- J. Lee, O. K. Farha, J. Roberts, K. A. Scheidt, S. T. Nguyen and J. T. Hupp, *Chem. Soc. Rev.*, 2009, **38**, 1450-1459.
- L. Ma, C. Abney and W. Lin, *Chem. Soc. Rev.*, 2009, **38**, 1248-1256.
- M. Yoon, R. Srirambalaji and K. Kim, *Chem. Rev.*, 2012, **112**, 1196-1231.
- J. Zhang, A. V. Biradar, S. Pramanik, T. J. Emge, T. Asefa and J. Li, *Chem. Commun.*, 2012, **48**, 6541-6543.
- H. R. Moon, D.-W. Lim and M. P. Suh, *Chem. Soc. Rev.*, 2013, **42**, 1807-1824.
- M. D. Allendorf, C. A. Bauer, R. K. Bhakta and R. J. T. Houk, *Chem. Soc. Rev.*, 2009, **38**, 1330-1352.
- B. Chen, S. Xiang and G. Qian, *Acc. Chem. Res.*, 2010, **43**, 1115-1124.
- Y. Cui, Y. Yue, G. Qian and B. Chen, *Chem. Rev.*, 2012, **112**, 1126-1162.
- L. E. Kreno, K. Leong, O. K. Farha, M. Allendorf, R. P. Van Duyne and J. T. Hupp, *Chem. Rev.*, 2012, **112**, 1105-1125.
- B. Liu, *J. Mater. Chem.*, 2012, **22**, 10094-10101.
- W. Zhang and R.-G. Xiong, *Chem. Rev.*, 2012, **112**, 1163-1195.
- C. Wang, T. Zhang and W. Lin, *Chem. Rev.*, 2012, **112**, 1084-1104.
- D. F. Sava, L. E. S. Rohwer, M. A. Rodriguez and T. M. Nenoff, *J. Am. Chem. Soc.*, 2012, **134**, 3983-3986.
- J.-C. Rybak, M. Hailmann, P. R. Matthes, A. Zurawski, J. Nitsch, A. Steffen, J. G. Heck, C. Feldmann, S. Götzendörfer, J. Meinhardt, G. Sextl, H. Kohlmann, S. J. Sedlmaier, W. Schnick and K. Müller-Buschbaum, *J. Am. Chem. Soc.*, 2013, **135**, 6896-6902.
- C.-Y. Sun, X.-L. Wang, X. Zhang, C. Qin, P. Li, Z.-M. Su, D.-X. Zhu, G.-G. Shan, K.-Z. Shao, H. Wu and J. Li, *Nat Commun.*, 2013, **4**.
- Y. Li, A. Pang, C. Wang and M. Wei, *J. Mater. Chem.*, 2011, **21**, 17259-17264.
- T. C. Narayan, T. Miyakai, S. Seki and M. Dincă, *J. Am. Chem. Soc.*, 2012, **134**, 12932-12935.
- A. Morozan and F. Jaouen, *Energy & Environmental Science*, 2012, **5**, 9269-9290.
- L. Sun, T. Miyakai, S. Seki and M. Dincă, *J. Am. Chem. Soc.*, 2013, **135**, 8185-8188.
- H. B. Wu, S. Wei, L. Zhang, R. Xu, H. H. Hng and X. W. Lou, *Chem. Eur. J.*, 2013, **19**, 10804-10808.
- G. K. H. Shimizu, J. M. Taylor and S. Kim, *Science*, 2013, **341**, 354-355.

37. P. Horcajada, T. Chalati, C. Serre, B. Gillet, C. Sebrie, T. Baati, J. F. Eubank, D. Heurtaux, P. Clayette, C. Kreuz, J.-S. Chang, Y. K. Hwang, V. Marsaud, P.-N. Bories, L. Cynober, S. Gil, G. Férey, P. Couvreur and R. Gref, *Nat Mater*, 2010, **9**, 172-178.
38. J. Della Rocca, D. Liu and W. Lin, *Acc. Chem. Res.*, 2011, **44**, 957-968.
39. P. Horcajada, R. Gref, T. Baati, P. K. Allan, G. Maurin, P. Couvreur, G. Férey, R. E. Morris and C. Serre, *Chem. Rev.*, 2012, **112**, 1232-1268.
40. D. J. Tranchemontagne, J. L. Mendoza-Cortes, M. O'Keefe and O. M. Yaghi, *Chem. Soc. Rev.*, 2009, **38**, 1257-1283.
41. J. Rocha, L. D. Carlos, F. A. A. Paz and D. Ananias, *Chem. Soc. Rev.*, 2011, **40**, 926-940.
42. S.-Z. Zhan, M. Li, X.-P. Zhou, J. Ni, X.-C. Huang and D. Li, *Inorg. Chem.*, 2011, **50**, 8879-8892.
43. Y. Kang, F. Wang, J. Zhang and X. Bu, *J. Am. Chem. Soc.*, 2012, **134**, 17881-17884.
44. M. Knorr, F. Guyon, A. Khatyr, C. Strohmann, M. Allain, S. M. Aly, A. Lapprand, D. Fortin and P. D. Harvey, *Inorg. Chem.*, 2012, **51**, 9917-9934.
45. J. Ni, K.-J. Wei, Y. Min, Y. Chen, S. Zhan, D. Li and Y. Liu, *Dalton Transactions*, 2012, **41**, 5280-5293.
46. X.-c. Shan, F.-l. Jiang, D.-q. Yuan, H.-b. Zhang, M.-y. Wu, L. Chen, J. Wei, S.-q. Zhang, J. Pan and M.-c. Hong, *Chem. Sci.*, 2013, **4**, 1484.
47. D. Zacher, O. Shekhah, C. Woll and R. A. Fischer, *Chem. Soc. Rev.*, 2009, **38**, 1418-1429.
48. O. Shekhah, J. Liu, R. A. Fischer and C. Woll, *Chem. Soc. Rev.*, 2011, **40**, 1081-1106.
49. J. R. Lakowicz, *Principles of Fluorescence Spectroscopy*, 3rd edn., Springer, 2006.
50. M. Sauer, J. Hofkens and J. Enderlein, *Handbook of Fluorescence Spectroscopy and Imaging: From Single Molecules to Ensembles*, Wiley-VCH Verlag GmbH & Co. KGaA, 2011.
51. N. B. Shustova, B. D. McCarthy and M. Dincă, *J. Am. Chem. Soc.*, 2011, **133**, 20126-20129.
52. J.-C. Dai, X.-T. Wu, Z.-Y. Fu, S.-M. Hu, W.-X. Du, C.-P. Cui, L.-M. Wu, H.-H. Zhang and R.-Q. Sun, *Chem. Commun.*, 2002, 12-13.
53. W. Chen, J.-Y. Wang, C. Chen, Q. Yue, H.-M. Yuan, J.-S. Chen and S.-N. Wang, *Inorg. Chem.*, 2003, **42**, 944-946.
54. G. A. Senchyk, V. O. Bukhan'ko, A. B. Lysenko, H. Krautscheid, E. B. Rusanov, A. N. Chernega, M. Karbowiak and K. V. Domasevitch, *Inorg. Chem.*, 2012, **51**, 8025-8033.
55. J. He, M. Zha, J. Cui, M. Zeller, A. D. Hunter, S.-M. Yiu, S.-T. Lee and Z. Xu, *J. Am. Chem. Soc.*, 2013, **135**, 7807-7810.
56. B. Manna, A. K. Chaudhari, B. Joarder, A. Karmakar and S. K. Ghosh, *Angew. Chem. Int. Ed.*, 2013, **52**, 998-1002.
57. Q. Tang, S. Liu, Y. Liu, J. Miao, S. Li, L. Zhang, Z. Shi and Z. Zheng, *Inorg. Chem.*, 2013, **52**, 2799-2801.
58. J.-S. Yang and T. M. Swager, *J. Am. Chem. Soc.*, 1998, **120**, 11864-11873.
59. S. J. Toal and W. C. Troglor, *J. Mater. Chem.*, 2006, **16**, 2871-2883.
60. J. C. Sanchez, A. G. DiPasquale, A. L. Rheingold and W. C. Troglor, *Chem. Mater.*, 2007, **19**, 6459-6470.
61. M. E. Germain and M. J. Knapp, *Chem. Soc. Rev.*, 2009, **38**, 2543-2555.
62. S. Pramanik, C. Zheng, X. Zhang, T. J. Emge and J. Li, *J. Am. Chem. Soc.*, 2011, **133**, 4153-4155.
63. J. Wang, J. Mei, W. Yuan, P. Lu, A. Qin, J. Sun, Y. Ma and B. Z. Tang, *J. Mater. Chem.*, 2011, **21**, 4056-4059.
64. S. Ramachandra, Z. D. Popovic', K. C. Schuermann, F. Cucinotta, G. Calzaferri and L. De Cola, *Small*, 2011, **7**, 1488-1494.
65. W. Wei, X. Huang, K. Chen, Y. Tao and X. Tang, *RSC Advances*, 2012, **2**, 3765-3771.
66. S. S. Nagarkar, B. Joarder, A. K. Chaudhari, S. Mukherjee and S. K. Ghosh, *Angew. Chem. Int. Ed.*, 2013, **52**, 2881-2885.
67. S. W. Thomas, G. D. Joly and T. M. Swager, *Chem. Rev.*, 2007, **107**, 1339-1386.
68. K. Jayaramulu, R. P. Narayanan, S. J. George and T. K. Maji, *Inorg. Chem.*, 2012, **51**, 10089-10091.
69. J.-x. Ma, X.-f. Huang, X.-q. Song and W.-s. Liu, *Chem. Eur. J.*, 2013, **19**, 3590-3595.
70. Z. Hu, S. Pramanik, K. Tan, C. Zheng, W. Liu, X. Zhang, Y. J. Chabal and J. Li, *Cryst. Growth Des.*, 2013, **13**, 4204-4207.
71. D. Banerjee, Z. Hu, S. Pramanik, X. Zhang, H. Wang and J. Li, *CrystEngComm*, 2013, **15**, 9745-9750.
72. S. Pramanik, Z. Hu, X. Zhang, C. Zheng, S. Kelly and J. Li, *Chem. Eur. J.*, 2013, **19**, 15964-15971.
73. B. Gole, A. K. Bar and P. S. Mukherjee, *Chem. Eur. J.*, 2014, **20**, 2276-2291.
74. N. B. Shustova, A. F. Cozzolino, S. Reineke, M. Baldo and M. Dincă, *J. Am. Chem. Soc.*, 2013, **135**, 13326-13329.
75. H. Xu, X. Rao, J. Gao, J. Yu, Z. Wang, Z. Dou, Y. Cui, Y. Yang, B. Chen and G. Qian, *Chem. Commun.*, 2012, **48**, 7377-7379.
76. Y. Li, S. Zhang and D. Song, *Angew. Chem. Int. Ed.*, 2013, **52**, 710-713.
77. C.-K. Lin, D. Zhao, W.-Y. Gao, Z. Yang, J. Ye, T. Xu, Q. Ge, S. Ma and D.-J. Liu, *Inorg. Chem.*, 2012, **51**, 9039-9044.
78. R. Sun, Y.-Z. Li, J. Bai and Y. Pan, *Cryst. Growth Des.*, 2007, **7**, 890-894.
79. X.-L. Wang, Y.-F. Bi, H.-Y. Lin and G.-C. Liu, *Cryst. Growth Des.*, 2007, **7**, 1086-1091.
80. Z. Tian, J. Lin, Y. Su, L. Wen, Y. Liu, H. Zhu and Q.-J. Meng, *Cryst. Growth Des.*, 2007, **7**, 1863-1867.
81. T. K. Kim, J. H. Lee, D. Moon and H. R. Moon, *Inorg. Chem.*, 2012, **52**, 589-595.
82. K. Jayaramulu, P. Kanoo, S. J. George and T. K. Maji, *Chem. Commun.*, 2010, **46**, 7906-7908.
83. P. L. Feng, K. Leong and M. D. Allendorf, *Dalton Transactions*, 2012, **41**, 8869-8877.
84. J.-H. Wang, M. Li and D. Li, *Chem. Sci.*, 2013, **4**, 1793-1801.
85. P. Wu, J. Wang, C. He, X. Zhang, Y. Wang, T. Liu and C. Duan, *Adv. Funct. Mater.*, 2012, **22**, 1698-1703.
86. S.-Z. Zhan, M. Li, S. W. Ng and D. Li, *Chem. Eur. J.*, 2013, **19**, 10217-10225.
87. J. Ferrando-Soria, H. Khajavi, P. Serra-Crespo, J. Gascon, F. Kapteijn, M. Julve, F. Lloret, J. Pasán, C. Ruiz-Pérez, Y. Journaux and E. Pardo, *Adv. Mater.*, 2012, **24**, 5625-5629.
88. Y.-Q. Lan, H.-L. Jiang, S.-L. Li and Q. Xu, *Adv. Mater.*, 2011, **23**, 5015-5020.
89. Y. Wang, J. Yang, Y.-Y. Liu and J.-F. Ma, *Chem. Eur. J.*, 2013, **19**, 14591-14599.
90. L. Han, L. Qin, L.-P. Xu and W.-N. Zhao, *Inorg. Chem.*, 2013, **52**, 1667-1669.
91. J. An, C. M. Shade, D. A. Chengelis-Czegán, S. Petoud and N. L. Rosi, *J. Am. Chem. Soc.*, 2011, **133**, 1220-1223.
92. H. Wang, W. Yang and Z.-M. Sun, *Chemistry – An Asian Journal*, 2013, **8**, 982-989.
93. M. Guo and Z.-M. Sun, *J. Mater. Chem.*, 2012, **22**, 15939-15946.
94. A. K. Chaudhari, S. S. Nagarkar, B. Joarder and S. K. Ghosh, *Cryst. Growth Des.*, 2013, **13**, 3716-3721.
95. G.-l. Liu, Y.-j. Qin, L. Jing, G.-y. Wei and H. Li, *Chem. Commun.*, 2013, **49**, 1699-1701.
96. A. Lan, K. Li, H. Wu, D. H. Olson, T. J. Emge, W. Ki, M. Hong and J. Li, *Angew. Chem. Int. Ed.*, 2009, **48**, 2334-2338.
97. A. M. Marti, S. D. Perera, L. D. McBeath and K. J. Balkus, *Langmuir*, 2013, **29**, 5927-5936.
98. Q. Zheng, F. Yang, M. Deng, Y. Ling, X. Liu, Z. Chen, Y. Wang, L. Weng and Y. Zhou, *Inorg. Chem.*, 2013, **52**, 10368-10374.
99. C.-C. Wang, C.-C. Yang, W.-C. Chung, G.-H. Lee, M.-L. Ho, Y.-C. Yu, M.-W. Chung, H.-S. Sheu, C.-H. Shih, K.-Y. Cheng, P.-J. Chang and P.-T. Chou, *Chem. Eur. J.*, 2011, **17**, 9232-9241.
100. J. Xiao, Y. Wu, M. Li, B.-Y. Liu, X.-C. Huang and D. Li, *Chem. Eur. J.*, 2013, **19**, 1891-1895.
101. Z.-J. Zhang, W. Shi, Z. Niu, H.-H. Li, B. Zhao, P. Cheng, D.-Z. Liao and S.-P. Yan, *Chem. Commun.*, 2011, **47**, 6425-6427.
102. F. Luo, G.-M. Sun, A.-m. Zheng, S.-x. Lian, Y.-l. Liu, X. F. Feng and Y.-y. Chu, *Dalton Transactions*, 2012, **41**, 13280-13283.
103. B. Gole, A. K. Bar and P. S. Mukherjee, *Chem. Commun.*, 2011, **47**, 12137-12139.

104. L. Chen, K. Tan, Y.-Q. Lan, S.-L. Li, K.-Z. Shao and Z.-M. Su, *Chem. Commun.*, 2012, **48**, 5919-5921.
105. Y.-Q. Lan, H.-L. Jiang, S.-L. Li and Q. Xu, *Inorg. Chem.*, 2012, **51**, 7484-7491.
106. F. Luo, M.-S. Wang, M.-B. Luo, G.-M. Sun, Y.-M. Song, P.-X. Li and G.-C. Guo, *Chem. Commun.*, 2012, **48**, 5989-5991.
107. D. Ma, B. Li, X. Zhou, Q. Zhou, K. Liu, G. Zeng, G. Li, Z. Shi and S. Feng, *Chem. Commun.*, 2013, **49**, 8964-8966.
108. Z. Jin, H. He, H. Zhao, T. Borjigin, F. Sun, D. Zhang and G. Zhu, *Dalton Transactions*, 2013, **42**, 13335-13338.
109. C.-C. Shen, W.-T. Chen and R.-S. Liu, *Dalton Transactions*, 2012, **41**, 11885-11888.
110. P. Kanoo, A. C. Ghosh, S. T. Cyriac and T. K. Maji, *Chem. Eur. J.*, 2012, **18**, 237-244.
111. J. Cui, Z. Lu, Y. Li, Z. Guo and H. Zheng, *Chem. Commun.*, 2012, **48**, 7967-7969.
112. S. Liu, Z. Xiang, Z. Hu, X. Zheng and D. Cao, *J. Mater. Chem.*, 2011, **21**, 6649-6653.
113. J. H. Lee, J. Jaworski and J. H. Jung, *Nanoscale*, 2013, **5**, 8533-8540.
114. Q.-B. Bo, H.-Y. Wang, D.-Q. Wang, Z.-W. Zhang, J.-L. Miao and G.-X. Sun, *Inorg. Chem.*, 2011, **50**, 10163-10177.
115. D. Liu, R. C. Huxford and W. Lin, *Angew. Chem.*, 2011, **123**, 3780-3784.
116. C. A. Kent, D. Liu, T. J. Meyer and W. Lin, *J. Am. Chem. Soc.*, 2012, **134**, 3991-3994.
117. Y.-T. Huang, Y.-C. Lai and S.-L. Wang, *Chem. Eur. J.*, 2012, **18**, 8614-8616.
118. K.-K. Yee, N. Reimer, J. Liu, S.-Y. Cheng, S.-M. Yiu, J. Weber, N. Stock and Z. Xu, *J. Am. Chem. Soc.*, 2013, **135**, 7795-7798.
119. W. Zhang, H. Huang, D. Liu, Q. Yang, Y. Xiao, Q. Ma and C. Zhong, *Microporous Mesoporous Mater.*, 2013, **171**, 118-124.
120. H.-L. Jiang, D. Feng, K. Wang, Z.-Y. Gu, Z. Wei, Y.-P. Chen and H.-C. Zhou, *J. Am. Chem. Soc.*, 2013, **135**, 13934-13938.
121. T. Lee, M. H. Tsai and H. L. Lee, *Cryst. Growth Des.*, 2012, **12**, 3181-3190.
122. C.-X. Chen, Q.-K. Liu, J.-P. Ma and Y.-B. Dong, *J. Mater. Chem.*, 2012, **22**, 9027-9033.
123. R. Li, Y.-P. Yuan, L.-G. Qiu, W. Zhang and J.-F. Zhu, *Small*, 2012, **8**, 225-230.
124. Q. Zhu, C. Shen, C. Tan, T. Sheng, S. Hu and X. Wu, *Chem. Commun.*, 2012, **48**, 531-533.
125. Q.-K. Liu, J.-P. Ma and Y.-B. Dong, *Chem. Commun.*, 2011, **47**, 7185-7187.
126. L. Sun, H. Xing, J. Xu, Z. Liang, J. Yu and R. Xu, *Dalton Transactions*, 2013, **42**, 5508-5513.
127. M. M. Wanderley, C. Wang, C.-D. Wu and W. Lin, *J. Am. Chem. Soc.*, 2012, **134**, 9050-9053.
128. H. Zhang, P. Lin, X. Shan, F. Du, Q. Li and S. Du, *Chem. Commun.*, 2013, **49**, 2231-2233.
129. T. Lee, Z. X. Liu and H. L. Lee, *Cryst. Growth Des.*, 2011, **11**, 4146-4154.
130. Y.-S. Xue, Y. He, L. Zhou, F.-J. Chen, Y. Xu, H.-B. Du, X.-Z. You and B. Chen, *J. Mater. Chem. A*, 2013, **1**, 4525-4530.
131. S. Dang, J.-H. Zhang and Z.-M. Sun, *J. Mater. Chem.*, 2012, **22**, 8868-8873.
132. M.-L. Ma, C. Ji and S.-Q. Zang, *Dalton Transactions*, 2013, **42**, 10579-10586.
133. Z. Amghouz, S. García-Granda, J. R. García, R. A. S. Ferreira, L. Mafta, L. D. Carlos and J. Rocha, *Inorg. Chem.*, 2011, **51**, 1703-1716.
134. S.-M. Li, X.-J. Zheng, D.-Q. Yuan, A. Ablet and L.-P. Jin, *Inorg. Chem.*, 2012, **51**, 1201-1203.
135. X. Rao, Q. Huang, X. Yang, Y. Cui, Y. Yang, C. Wu, B. Chen and G. Qian, *J. Mater. Chem.*, 2012, **22**, 3210-3214.
136. L.-N. Jia, L. Hou, L. Wei, X.-J. Jing, B. Liu, Y.-Y. Wang and Q.-Z. Shi, *Cryst. Growth Des.*, 2013, **13**, 1570-1576.
137. H.-Y. Gong, B. M. Rambo, C. A. Nelson, V. M. Lynch, X. Zhu and J. L. Sessler, *Chem. Commun.*, 2012, **48**, 10186-10188.
138. H. Xu, F. Liu, Y. Cui, B. Chen and G. Qian, *Chem. Commun.*, 2011, **47**, 3153-3155.
139. S. Dang, E. Ma, Z.-M. Sun and H. Zhang, *J. Mater. Chem.*, 2012, **22**, 16920-16926.
140. Z. Hao, X. Song, M. Zhu, X. Meng, S. Zhao, S. Su, W. Yang, S. Song and H. Zhang, *J. Mater. Chem. A*, 2013, **1**, 11043-11050.
141. X.-H. Zhou, L. Li, H.-H. Li, A. Li, T. Yang and W. Huang, *Dalton Transactions*, 2013, **42**, 12403-12409.
142. X. Zhou, H. Li, H. Xiao, L. Li, Q. Zhao, T. Yang, J. Zuo and W. Huang, *Dalton Transactions*, 2013, **42**, 5718-5723.
143. M. Zheng, H. Tan, Z. Xie, L. Zhang, X. Jing and Z. Sun, *ACS Applied Materials & Interfaces*, 2013, **5**, 1078-1083.
144. Y.-M. Zhu, C.-H. Zeng, T.-S. Chu, H.-M. Wang, Y.-Y. Yang, Y.-X. Tong, C.-Y. Su and W.-T. Wong, *J. Mater. Chem. A*, 2013, **1**, 11312-11319.
145. J.-K. Sun, L.-X. Cai, Y.-J. Chen, Z.-H. Li and J. Zhang, *Chem. Commun.*, 2011, **47**, 6870-6872.
146. A. Zurawski, M. Mai, D. Baumann, C. Feldmann and K. Muller-Buschbaum, *Chem. Commun.*, 2011, **47**, 496-498.
147. Y. Liu, M. Pan, Q.-Y. Yang, L. Fu, K. Li, S.-C. Wei and C.-Y. Su, *Chem. Mater.*, 2012, **24**, 1954-1960.
148. J.-M. Zhou, W. Shi, N. Xu and P. Cheng, *Inorg. Chem.*, 2013, **52**, 8082-8090.
149. S.-R. Zhang, D.-Y. Du, K. Tan, J.-S. Qin, H.-Q. Dong, S.-L. Li, W.-W. He, Y.-Q. Lan, P. Shen and Z.-M. Su, *Chem. Eur. J.*, 2013, **19**, 11279-11286.
150. S. Dang, J.-H. Zhang, Z.-M. Sun and H. Zhang, *Chem. Commun.*, 2012, **48**, 11139-11141.
151. R. F. D'Vries, S. Alvarez-Garcia, N. Snejko, L. E. Bausa, E. Gutierrez-Puebla, A. de Andres and M. A. Monge, *J. Mater. Chem. C*, 2013, **1**, 6316-6324.
152. P. R. Matthes, C. J. Holler, M. Mai, J. Heck, S. J. Sedlmaier, S. Schmiechen, C. Feldmann, W. Schnick and K. Muller-Buschbaum, *J. Mater. Chem.*, 2012, **22**, 10179-10187.
153. Y. Yu, J.-P. Ma and Y.-B. Dong, *CrystEngComm*, 2012, **14**, 7157-7160.
154. I. T. v. Weber, A. J. G. de Melo, M. A. d. M. Lucena, M. O. Rodrigues and S. Alves Junior, *Anal. Chem.*, 2011, **83**, 4720-4723.
155. H. Li, W. Shi, K. Zhao, Z. Niu, H. Li and P. Cheng, *Chem. Eur. J.*, 2013, **19**, 3358-3365.
156. P. Wu, J. Wang, Y. Li, C. He, Z. Xie and C. Duan, *Adv. Funct. Mater.*, 2011, **21**, 2788-2794.
157. J.-D. Xiao, L.-G. Qiu, F. Ke, Y.-P. Yuan, G.-S. Xu, Y.-M. Wang and X. Jiang, *J. Mater. Chem. A*, 2013, **1**, 8745-8752.
158. B. Liu and Y. Chen, *Anal. Chem.*, 2013, **85**, 11020-11025.
159. H. Yang, F. Wang, Y.-X. Tan, Y. Kang, T.-H. Li and J. Zhang, *Chemistry – An Asian Journal*, 2012, **7**, 1069-1073.
160. X. Rao, T. Song, J. Gao, Y. Cui, Y. Yang, C. Wu, B. Chen and G. Qian, *J. Am. Chem. Soc.*, 2013, **135**, 15559-15564.
161. A. Cadiou, C. D. S. Brites, P. M. F. J. Costa, R. A. S. Ferreira, J. Rocha and L. D. Carlos, *ACS Nano*, 2013, **7**, 7213-7218.
162. Y. Cui, H. Xu, Y. Yue, Z. Guo, J. Yu, Z. Chen, J. Gao, Y. Yang, G. Qian and B. Chen, *J. Am. Chem. Soc.*, 2012, **134**, 3979-3982.
163. Z. Guo, H. Xu, S. Su, J. Cai, S. Dang, S. Xiang, G. Qian, H. Zhang, M. O'Keeffe and B. Chen, *Chem. Commun.*, 2011, **47**, 5551-5553.
164. L. Li, S. Zhang, L. Han, Z. Sun, J. Luo and M. Hong, *Cryst. Growth Des.*, 2012, **13**, 106-110.
165. X.-P. Zhang, D.-G. Wang, Y. Su, H.-R. Tian, J.-J. Lin, Y.-L. Feng and J.-W. Cheng, *Dalton Transactions*, 2013, **42**, 10384-10387.
166. J.-R. Li, J. Yu, W. Lu, L.-B. Sun, J. Sculley, P. B. Balbuena and H.-C. Zhou, *Nat Commun*, 2013, **4**, 1538.
167. B. Chen, L. Wang, Y. Xiao, F. R. Fronczek, M. Xue, Y. Cui and G. Qian, *Angew. Chem. Int. Ed.*, 2009, **48**, 500-503.
168. B. Chen, Y. Yang, F. Zapata, G. Lin, G. Qian and E. B. Lobkovsky, *Adv. Mater.*, 2007, **19**, 1693-1696.
169. B. Chen, L. Wang, F. Zapata, G. Qian and E. B. Lobkovsky, *J. Am. Chem. Soc.*, 2008, **130**, 6718-6719.
170. C. H. Hendon, D. Tiana, M. Fontecave, C. Sanchez, L. D'arras, C. Sassoey, L. Rozes, C. Mellot-Draznieks and A. Walsh, *J. Am. Chem. Soc.*, 2013, **135**, 10942-10945.
171. G. Long and M. E. Meek, *J. Environ. Sci. Health Part C*, 2001, **19**, 161-187.
172. D. Rui, C. Daojun and Y. Yongjian, *Environ. Toxicol. Pharmacol.*, 2011, **31**, 357-363.

173. H.-L. Jiang, D. Feng, T.-F. Liu, J.-R. Li and H.-C. Zhou, *J. Am. Chem. Soc.*, 2012, **134**, 14690-14693.
174. D. Feng, Z.-Y. Gu, J.-R. Li, H.-L. Jiang, Z. Wei and H.-C. Zhou, *Angew. Chem. Int. Ed.*, 2012, **51**, 10307-10310.
175. M. L. Cable, J. P. Kirby, K. Sorasaene, H. B. Gray and A. Ponce, *J. Am. Chem. Soc.*, 2007, **129**, 1474-1475.
176. W. J. Rieter, K. M. L. Taylor and W. Lin, *J. Am. Chem. Soc.*, 2007, **129**, 9852-9853.
177. K. M. L. Taylor and W. Lin, *J. Mater. Chem.*, 2009, **19**, 6418-6422.
178. M. L. Cable, J. P. Kirby, D. J. Levine, M. J. Manary, H. B. Gray and A. Ponce, *J. Am. Chem. Soc.*, 2009, **131**, 9562-9570.
179. W.-H. Zhu, Z.-M. Wang and S. Gao, *Inorg. Chem.*, 2007, **46**, 1337-1342.
180. X. Wei, L. Zheng, F. Luo, Z. Lin, L. Guo, B. Qiu and G. Chen, *J. Mater. Chem. B*, 2013, **1**, 1812-1817.
181. T. Nagano and T. Yoshimura, *Chem. Rev.*, 2002, **102**, 1235-1270.
182. K. G. Furton and L. J. Myers, *Talanta*, 2001, **54**, 487-500.
183. E. Wallis, T. M. Griffin, J. N. Popkie, M. A. Eagan, R. F. McAtee, D. Vrazel and J. McKinly, 2005.
184. K. Håkansson, R. V. Coorey, R. A. Zubarev, V. L. Talrose and P. Håkansson, *J. Mass Spectrom.*, 2000, **35**, 337-346.
185. J. M. Sylvia, J. A. Janni, J. D. Klein and K. M. Spencer, *Anal. Chem.*, 2000, **72**, 5834-5840.
186. R. D. Luggar, M. J. Farquharson, J. A. Horrocks and R. J. Lacey, *X-Ray Spectrom.*, 1998, **27**, 87-94.
187. S. F. Hollowell, *Talanta*, 2001, **54**, 447-458.
188. Y. Salinas, R. Martinez-Manez, M. D. Marcos, F. Sancenon, A. M. Costero, M. Parra and S. Gil, *Chem. Soc. Rev.*, 2012, **41**, 1261-1296.
189. D. Gopalakrishnan and W. R. Dichtel, *J. Am. Chem. Soc.*, 2013, **135**, 8357-8362.
190. R. L. Woodfin, *Trace Chemical Sensing of Explosives*, John Wiley & Sons, 2006.
191. F. Terrier, *Chem. Rev.*, 1982, **82**, 77-152.
192. G. A. Artamkina, M. P. Egorov and I. P. Beletskaya, *Chem. Rev.*, 1982, **82**, 427-459.
193. K. Zhang, H. Zhou, Q. Mei, S. Wang, G. Guan, R. Liu, J. Zhang and Z. Zhang, *J. Am. Chem. Soc.*, 2011, **133**, 8424-8427.
194. T. L. Andrew and T. M. Swager, *J. Am. Chem. Soc.*, 2007, **129**, 7254-7255.
195. *US Pat.*, US7666684 B2, 2010.
196. T. L. Andrew and T. M. Swager, *J. Org. Chem.*, 2011, **76**, 2976-2993.
197. J. C. Sanchez and W. C. Trogler, *J. Mater. Chem.*, 2008, **18**, 3143-3156.
198. J. C. Sanchez, S. A. Urbas, S. J. Toal, A. G. DiPasquale, A. L. Rheingold and W. C. Trogler, *Macromolecules*, 2008, **41**, 1237-1245.
199. M. J. Frisch, G. W. Trucks, H. B. Schlegel, G. E. Scuseria, M. A. Robb, J. R. Cheeseman, G. Scalmani, V. Barone, B. Mennucci, G. A. Petersson, H. Nakatsuji, M. Caricato, X. Li, H. P. Hratchian, A. F. Izmaylov, J. Bloino, G. Zheng, J. L. Sonnenberg, M. Hada, M. Ehara, K. Toyota, R. Fukuda, J. Hasegawa, M. Ishida, T. Nakajima, Y. Honda, O. Kitao, H. Nakai, T. Vreven, J. J. A. Montgomery, J. E. Peralta, F. Ogliaro, M. Bearpark, J. J. Heyd, E. Brothers, K. N. Kudin, V. N. Staroverov, T. Keith, R. Kobayashi, J. Normand, K. Raghavachari, A. Rendell, J. C. Burant, S. S. Iyengar, J. Tomasi, M. Cossi, N. Rega, J. M. Millam, M. Klene, J. E. Knox, J. B. Cross, V. Bakken, C. Adamo, J. Jaramillo, R. Gomperts, R. E. Stratmann, O. Yazyev, A. J. Austin, R. Cammi, C. Pomelli, J. W. Ochterski, R. L. Martin, K. Morokuma, V. G. Zakrzewski, G. A. Voth, P. Salvador, J. J. Dannenberg, S. Dapprich, A. D. Daniels, O. Farkas, J. B. Foresman, J. V. Ortiz, J. Cioslowski and D. J. Fox, Gaussian 09, Revision C.01, Gaussian, Inc., Wallingford CT, 2010.
200. Z. Hu, K. Tan, H. Wang, Y. Zhao, C. Zheng, D. Banerjee, Q. Gong, T. J. Emge, Y. J. Chabal and J. Li, 2014, **Submitted**.
201. A. Lan, K. Li, H. Wu, L. Kong, N. Nijem, D. H. Olson, T. J. Emge, Y. J. Chabal, D. C. Langreth, M. Hong and J. Li, *Inorg. Chem.*, 2009, **48**, 7165-7173.
202. N. B. Shustova, T.-C. Ong, A. F. Cozzolino, V. K. Michaelis, R. G. Griffin and M. Dincă, *J. Am. Chem. Soc.*, 2012, **134**, 15061-15070.
203. N. B. Shustova, A. F. Cozzolino and M. Dincă, *J. Am. Chem. Soc.*, 2012, **134**, 19596-19599.
204. B. Chen, S. Ma, F. Zapata, E. B. Lobkovsky and J. Yang, *Inorg. Chem.*, 2006, **45**, 5718-5720.
205. R. Xiong, J. T. Fern, D. J. Keffer, M. Fuentes-Cabrera and D. M. Nicholson, *Molecular Simulation*, 2009, **35**, 910-919.
206. K. Odbadrakh, J. P. Lewis, D. M. Nicholson, T. Petrova, A. Michalkova and J. Leszczynski, *The Journal of Physical Chemistry C*, 2010, **114**, 3732-3736.
207. R. Xiong, D. J. Keffer, M. Fuentes-Cabrera, D. M. Nicholson, A. Michalkova, T. Petrova, J. Leszczynski, K. Odbadrakh, B. L. Doss and J. P. Lewis, *Langmuir*, 2010, **26**, 5942-5950.
208. R. Xiong, K. Odbadrakh, A. Michalkova, J. P. Luna, T. Petrova, D. J. Keffer, D. M. Nicholson, M. A. Fuentes-Cabrera, J. P. Lewis and J. Leszczynski, *Sensors and Actuators B: Chemical*, 2010, **148**, 459-468.
209. M. Ji, X. Lan, Z. Han, C. Hao and J. Qiu, *Inorg. Chem.*, 2012, **51**, 12389-12394.
210. M. Ji, C. Hao, D. Wang, H. Li and J. Qiu, *Dalton Transactions*, 2013, **42**, 3464-3470.
211. X. Sui, M. Ji, X. Lan, W. Mi, C. Hao and J. Qiu, *Inorg. Chem.*, 2013, **52**, 5742-5748.
212. C. Zhang, Y. Che, Z. Zhang, X. Yang and L. Zang, *Chem. Commun.*, 2011, **47**, 2336-2338.
213. J. R. Cox, P. Müller and T. M. Swager, *J. Am. Chem. Soc.*, 2011, **133**, 12910-12913.
214. M. A. Ivy, L. T. Gallagher, A. D. Ellington and E. V. Anslyn, *Chem. Sci.*, 2012, **3**, 1773-1779.